

This work was written as part of one of the author's official duties as an Employee of the United States Government and is therefore a work of the United States Government. In accordance with 17 U.S.C. 105, no copyright protection is available for such works under U.S. Law.

Public Domain Mark 1.0

<https://creativecommons.org/publicdomain/mark/1.0/>

Access to this work was provided by the University of Maryland, Baltimore County (UMBC) ScholarWorks@UMBC digital repository on the Maryland Shared Open Access (MD-SOAR) platform.

**Please provide feedback**

Please support the ScholarWorks@UMBC repository by emailing [scholarworks-group@umbc.edu](mailto:scholarworks-group@umbc.edu) and telling us what having access to this work means to you and why it's important to you. Thank you.

# Use of the Ångström exponent to estimate the variability of optical and physical properties of aging smoke particles in Brazil

Jeffrey S. Reid,<sup>1</sup> Thomas F. Eck,<sup>2</sup> Sundar A. Christopher,<sup>3</sup>  
Peter V. Hobbs,<sup>4</sup> and Brent Holben<sup>5</sup>

**Abstract.** In situ airborne measurements from the Smoke, Clouds and Radiation-Brazil (SCAR-B) study show that during aging over 1–4 days the physical and optical properties of smoke particles are correlated. Consequently, if one optical or physical property of the smoke particles is determined, other properties can be derived. This methodology is validated using multiwavelength Ångström exponents determined from the ground-based Sun photometer measurements in SCAR-B. It is shown that the Ångström exponent determined from Sun photometers for the wavelength intervals 339–437 nm and 437–669 nm are well correlated with particle size, single-scattering albedo, and the backscatter ratio ( $r^2 > 0.8$ ). Therefore, when almucantar sky radiance data are not available and for remote sensing applications (such as MODIS), some of the uncertainties in the properties of smoke particles can be reduced by applying these relationships. Using this methodology, major oscillations were observed in smoke particle properties in Brazil on timescales of ~5–15 days, resulting in variations of the volume median diameter and single-scattering albedo of  $\pm 0.04 \mu\text{m}$  and  $\pm 0.05$ , respectively. In comparison, the mean value of the dry smoke particle volume median diameter and single-scattering albedo over all of Brazil was  $0.27 \mu\text{m}$  and  $0.86$ , respectively. A daily cycle in smoke particle properties was also observed. The weekly and seasonal variability in the single-scattering albedo is shown to have significant consequences for retrieving aerosol optical depths from satellite measurements.

## 1. Introduction

Smoke particles from biomass burning change rapidly in size and composition after being emitted into the atmosphere [Westphal and Toon, 1991; Lioussé et al., 1995; Radke et al., 1995; Hobbs et al., 1997a; Reid et al., 1998a]. Consequently, measurements of the physical, chemical, and optical properties of smoke particles very close to fires may not adequately represent their properties in dispersed and aged smoke plumes. If the evolution of smoke particles as they age is not properly accounted for, large errors may result in calculations of their radiative forcing on regional and global scales.

Biomass burning in the tropical broadleaf and cerrado forested regions of Brazil creates a smoky haze that covers much of the South American continent from August through September [Artaxo et al., 1994; Holben et al., 1996; Prins et al., 1998]. In this subcontinental scale plume, particle coagulation, gas-to-particle conversion, heterogeneous reactions in hazes, and cloud processing, influence the size distribution of the

particles [Reid et al., 1998a]. These processes can increase the mass scattering efficiency ( $\alpha_s$ ) of the smoke particles at mid-visible wavelengths from  $\sim 3.3$  to  $4.2 \text{ m}^2 \text{ g}^{-1}$ , increase the single-scattering albedo ( $\omega_0$ ) from  $\sim 0.79$  to  $\sim 0.90$ , decrease the backscatter ratio ( $\beta(1)$ ) of the particles from  $0.17$  to  $0.11$ , and cause the Ångström exponent to decrease as the particles age [Reid et al., 1998a].

Because the evolutionary processes that influence smoke particles are strongly dependent on environmental variables (e.g., smoke concentration, cloud cover, relative humidity, etc.), significant particle growth can occur on timescales varying from hours to days [Reid et al., 1998a]. This makes it difficult to determine appropriate values of the parameters required for modeling the radiative effects of smoke particles on regional and global scales. Christopher et al. [1999] showed that use of regional mean values of  $\omega_0$  and the asymmetry parameter ( $g$ ) for smoke particles in Brazil can result in errors as large as  $95 \text{ W m}^{-2}$  in the modeling of downward shortwave radiative fluxes at the surface. Therefore it is important to account for the effects of particle aging.

During August and September 1995 the Smoke, Clouds, and Radiation-Brazil (SCAR-B) field project was conducted to study smoke from biomass burning in Brazil [Kaufman et al., 1998]. One of the main goals of SCAR-B was to obtain measurements of the physical, chemical, and radiative properties of the palls of smoke that cover millions of square kilometers of the Amazon Basin and the cerrado regions of Brazil during the biomass burning season. During the SCAR-B field study, 15 Aerosol Robotic Network (AERONET) Sun photometers were deployed across Brazil to measure aerosol optical thick-

<sup>1</sup>Tropospheric Branch-D883, Space and Naval Warfare System Center, San Diego, California.

<sup>2</sup>Raytheon RITSS Corporation, NASA Goddard Space Flight Center, Greenbelt, Maryland.

<sup>3</sup>Department of Atmospheric Science, University of Alabama in Huntsville.

<sup>4</sup>Department of Atmospheric Sciences, University of Washington, Seattle.

<sup>5</sup>NASA Goddard Space Flight Center, Greenbelt, Maryland.

Copyright 1999 by the American Geophysical Union.

Paper number 1999JD900833.  
0148-0227/99/1999JD900833\$09.00

nesses (AOT) and sky radiances for time periods ranging from 3 days to 4 months. Also participating in SCAR-B was the University of Washington's (UW) Cloud and Aerosol Research Group with its Convair C-131A research aircraft.

One of the findings from measurements made aboard the UW C-131A aircraft in SCAR-B was that although smoke particles can grow rapidly, the count median diameter (CMD), volume median diameter (VMD), and geometric standard deviation of their particle size distributions are generally fairly well correlated ( $r^2 \approx 0.7$ ) [Reid et al., 1998a]. Particle optical properties were also correlated ( $r^2 \approx 0.5$ ). Reid et al. suggested that if just one optical property of the particles is measured (say the backscatter ratio or Ångström exponent), then some of the other properties of the particles, such as particle size distribution parameters and single-scattering albedo, can be deduced. In this paper we test this suggestion by correlating particle parameters derived from the AERONET and UW C-131A measurements in SCAR-B. Relationships are presented between the Ångström exponent, derived from Sun photometer AOT measurements and in situ measurements of smoke particle size,  $\omega_0$  and  $\beta(1)$  obtained aboard the UW C-131A. Using the Ångström exponent allows estimation of key optical parameters needed to model the aerosol radiative forcing. By analyzing the variability of the Ångström exponent at three AERONET Sun photometer sites, we determine the timescales and length scales over which variations occur in particle properties and estimate the uncertainty that these variations introduce in radiative transfer calculations.

## 2. The Ångström Exponent

Aerosol optical thickness (AOT) is the integral of atmospheric extinction coefficient  $\sigma_e$  from the surface to the top of the atmosphere. The spectral dependence of the AOT is frequently parameterized through the particle Ångström exponent ( $\alpha$ ) which is computed from the Ångström [1929] relation:

$$\tau_a = \tau_o \lambda^{-\alpha}, \quad (1)$$

where  $\tau_a$  is the AOT,  $\lambda$  the wavelength (in  $\mu\text{m}$ ), and  $\tau_o$  the optical depth at  $\lambda = 1 \mu\text{m}$ . Because the wavelength dependence of the AOT does not follow (1) exactly,  $\alpha$  can be computed for any subrange using the expression:

$$\alpha = -\frac{\ln(\tau_{a1}/\tau_{a2})}{\ln(\lambda_1/\lambda_2)}, \quad (2)$$

where  $\tau_{a1}$  and  $\tau_{a2}$  are the AOT at wavelengths of  $\lambda_1$  and  $\lambda_2$ , respectively. As particles increase in size, the value of  $\alpha$  decreases. For example,  $\alpha$  is  $\sim 0$  for coarse-mode soil particles, and  $\alpha$  is 1 to 3 for fine-mode anthropogenic pollutants [Tanré et al., 1988; Nakajima et al., 1989; Tomasi et al., 1983].

The Ångström exponent can be related to the Junge [1955] distribution:

$$\frac{dN}{d(\ln r)} = c \cdot r^{-\nu}, \quad (3)$$

where  $dN$  is the number concentration of particles with radii between  $r$  and  $r + dr$ , and  $c$  and  $\nu$  are fitting parameters. For particles in the size range  $0.1 \mu\text{m} < r < 1 \mu\text{m}$ ,  $\alpha \approx \nu - 2$  [Tomasi et al., 1983]. However, this relationship between  $\alpha$  and  $\nu$  does not apply to all aerosol types [Tomasi et al., 1983; Dellago and Horvath, 1993].

Particles in smoky hazes over Brazil tend to display a single

submicron mode, with CMD and VMD of  $\sim 0.12$ – $0.25 \mu\text{m}$  and  $\sim 0.25$ – $0.34 \mu\text{m}$ , respectively [Reid et al., 1998a]. In this size range a strong relationship is expected between  $\alpha$  and  $\nu$  [Tomasi et al., 1983]. However, it has been suggested that a soil mode is sometimes present in the aerosol over the Amazon Basin [Artaxo et al., 1994; Remer et al., 1998], which could reduce the relationship between  $\alpha$  and  $\nu$ .

Reid et al. [1998a] found that the Ångström exponent of smoke particles in Brazil ranged from 2.5 for fresh smoke to as low as 0.5 for well-aged smoke. They also found that as expected,  $\alpha$  decreased as the fine-mode particle size increased. Therefore, although there is not a unique relationship between  $\alpha$  and  $\nu$  for all submicron mode pollutants, for a single fine-mode aerosol type, such as that produced by biomass burning,  $\alpha$  can be a useful indicator of changes in  $\nu$  and therefore the size distribution of the smoke particles.

## 3. Methods

For a complete description of the SCAR-B experiment and a summary of its findings the reader is referred to Kaufman et al. [1998]. Details on the AERONET Sun photometers deployed in SCAR-B are given by Eck et al. [1998]. A list of UW C-131A flights and instrumentation in SCAR-B can be found in the work of P. V. Hobbs (Summary of types of data collected on the University of Washington's Convair C-131A aircraft in the Smoke, Clouds and Radiation-Brazil (SCAR-B) field study from 17 August–20 September 1995, available at <http://cargsun2.atmos.washington.edu>). A brief description of the instruments that provided data used in this paper follows.

### 3.1. AERONET Sun Photometer Data

During SCAR-B, AOT measurements were made from 15 AERONET Sun photometer sites in Brazil, which were deployed from 3 days to 4 months. An advanced very high resolution radiometer (AVHRR) image showing the typical position of the subcontinental pall of smoke with respect to these sites is shown in Figure 1. All of the sites had automatic sun and sky scanning radiometers that made direct sun measurements at wavelengths of 339, 379, 437, 498, 669, 871, 940, and 1021 nm every 15 min in a  $0.8^\circ$  field of view [Holben et al., 1998]. In this study, all but the 379 and 940 nm channels were used to compute AOT (the 379 nm channel had significant “out of bandpass leakage” from other wavelengths, and the 940 nm channel was used to compute precipitable water vapor). The 339 nm channel had a 2.5 nm bandpass filter, and the 437, 498, 669, 871, and 1021 nm channels had 10 nm bandpass filters. Cloud screening was performed using the method described by Smirnov et al. [1999]. Values for  $\alpha$  were computed for the bandwidth intervals 338–437 nm, 437–669 nm, 498–871 nm, and 338–1021 nm by performing a power law fit of  $\tau(\lambda)$  versus  $\lambda$ . There was no statistical difference between  $\alpha$  computed using a power law fit and equation (2).

Almucantar sky radiance measurements were made at wavelengths of 437, 669, 871, and 1021 nm when the solar zenith angle was greater than  $60^\circ$  (early morning and late afternoon). From these measurements, the scattering phase function and particle size distribution can be retrieved using the methodology described by Nakajima et al. [1996]. However, this method introduces large errors when multiple scattering occurs (e.g., when the optical depth approaches or exceeds 1). Since optical depths in Brazil during the burning season are frequently in excess of 1, retrieval of phase functions and particle size dis-

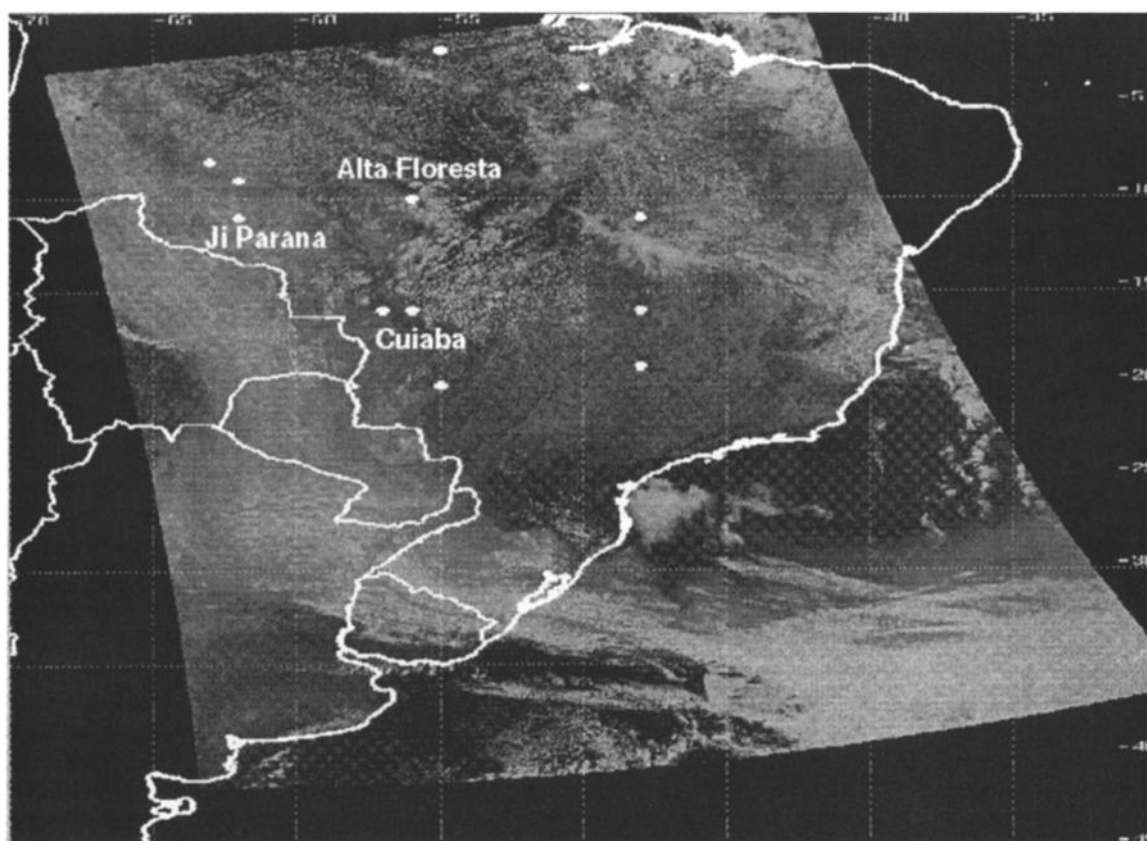


**Figure 1.** Advanced very high resolution radiometer (AVHRR) channel 1 imagery of South America at the middle (September 1, 1995) of the SCAR-B field study. Smoke is visible in the  $-5^{\circ}$  to  $-18^{\circ}$  latitude band, as well as being advected south along the  $60^{\circ}$  longitude line. Sun photometer sites during SCAR-B are marked as white dots.

tributions using the method described by Nakajima et al. are not viable for most of the SCAR-B data set. Additionally, because there were no UW C-131A vertical profiles over the Sun photometer sites in the early morning and late afternoon, these data were not used in the present study.

### 3.2. UW C-131A Aircraft

In SCAR-B the UW C-131A aircraft was used to study a wide variety of regional hazes dominated by smoke in Brazil from August 23 through September 18, 1995. Flight operations were conducted from three principal bases: Cuiabá (in the state of Mato Grosso,  $16^{\circ}\text{S}$ ,  $56^{\circ}\text{W}$ ), Porto Velho (Rondonia,  $9^{\circ}\text{S}$ ,  $64^{\circ}\text{W}$ ), and Marabá (Pará,  $5^{\circ}\text{S}$ ,  $49^{\circ}\text{W}$ ). A map showing the locations of these sites is given by Kaufman et al. [1998]. Cuiabá is in the cerrado (grass and shrub plains) region, and Porto Velho and Marabá are, respectively, in the western and eastern portions of the tropical forested portions of the Amazon Basin.

Light-scattering measurements were obtained on the UW C-131A with a three-wavelength nephelometer ( $\lambda = 450, 550, 700 \text{ nm}$ ) built by MS Electron Incorporated [Hegg et al., 1996]. Aerosols were sampled continuously through a pressure-regulated, isokinetic inlet (size cutpoint of  $\sim 4 \mu\text{m}$ ) and were dried to a relative humidity  $< 35\%$ . The nephelometer had a backscatter shutter to determine total hemispheric backscattering ( $\theta$  between  $90^{\circ}$  and  $170^{\circ}$ ) and the hemispherical backscatter ratio,  $\beta(1)$ , was computed from

$$\beta(1) = \frac{\int_{\pi/2}^{\pi} \bar{P} \sin(\theta) d\theta}{\int_0^{\pi} \bar{P} \sin(\theta) d\theta}. \quad (4)$$

For particles  $< 0.6 \mu\text{m}$  diameter (typical of this study) the truncation errors in the  $3\text{-}\lambda$  nephelometer were small and were accounted for in part. To mitigate the errors produced by a non-Lambertian light source, the lamp in the nephelometer used in the present study was fitted with a special ground glass window. We estimate that the truncation and light source errors produced a  $\pm 3\%$  uncertainty in the scattering measurements of fine-mode aerosols.

Ångström exponents were calculated from the light-scattering coefficients measured with the  $3\text{-}\lambda$  nephelometer:

$$\alpha = - \frac{\ln(\sigma_{s1}/\sigma_{s2})}{\ln(\lambda_1/\lambda_2)}. \quad (5)$$

The Ångström exponent determined in this way was not corrected for particle hygroscopicity. Kotchenruther and Hobbs [1998] found that the hygroscopic growth factor for the aged smoke in Cuiabá and Porto Velho to be small ( $\sim 1.15$ ), and they did not detect any wavelength dependence. Since  $\alpha$  de-

**Table 1.** Summary of the UW C-131A Flights and Sun Photometer Sites Used in This Study

Sun Photometer Site	UW Flight Number	Date (1995)	Time, UTC	Full Vertical Profile	AOT ( $\lambda = 498$ nm)	$\omega_0$ ( $\lambda = 550$ nm)	CMD, $\mu\text{m}$
Cuiabá	1692	Aug. 24	1630	yes	0.2	0.80	0.10
Cuiabá	1693	Aug. 25	1730	no	0.5	0.81	0.16
Cuiabá	1694	Aug. 27	1945	yes	0.9	0.81	0.18
Cuiabá	1695	Aug. 28	1940	no	0.5	0.80	0.12
Pantanal	1696	Aug. 30	1500	yes	2.2	0.87	0.23
Pantanal	1697	Sept. 1	1300	yes	1.9	0.84	0.21
Cuiabá	1698	Sept. 4	1450	no	0.6	0.83	0.18
Jamari/Pototsi Mine/Repressa Sammuel	1700	Sept. 5	2000	yes	2.8	0.88	0.20
Jamari/Pototsi Mine/Repressa Sammuel	1701	Sept. 6	1300	yes	2.1	0.86	0.20
Jamari/Pototsi Mine/Repressa Sammuel	1703	Sept. 7	1700	yes	1.7	0.87	0.20

Also listed are the aerosol optical thickness (AOT) from the Sun photometer sites, the single-scattering albedo ( $\omega_0$ ), and the particle count median diameter (CMD) measured on the UW C-131A.

depends only on the ratio of the light-scattering coefficients, the hygroscopic growth factor drops out of (5).

Continuous absorption measurements were made on the same inlet as the nephelometer using a Particle Soot/Absorption Photometer (PSAP), manufactured by Radiance Research. The PSAP operated at a wavelength of 550 nm and used a quartz filter substrate. The integration time for each data point was 1 min. Reid *et al.* [1998b] describes how the PSAP performed relative to the other methods used to measure absorption in SCAR-B. For one flight (UW 1698), PSAP data were unavailable; in this case, the absorption measurements were made by using the integrating plate method [Reid *et al.*, 1998b].

Combination of  $\sigma_a$  from the PSAP with  $\sigma_s$  from the 3- $\lambda$  nephelometer yielded the single-scattering albedo  $\omega_0$  at 550 nm. The single-scattering albedo was corrected for hygroscopicity by assuming that changes in relative humidity affected only  $\sigma_s$ . Because particle hygroscopicities were small, this correction increased  $\omega_0$  by no more than 0.015.

Continuous particle sizing measurements were made on the UW C-131A aircraft using a Passive Cavity Aerosol Spectrometer Probe (PCASP-100X) mounted on the wing. The PCASP-100X measured dried aerosol particles with diameters from 0.1 to 3  $\mu\text{m}$ . For this instrument, there are sizing errors for particles having indices of refraction that differ from those of the latex spheres used for its calibration ( $n = 1.59 - 0i$ ). To compensate for this, the PCASP response curve was optimized [Pueschel *et al.*, 1990] for particles with indices of refraction of  $1.5 - 0.02i$  using the closure calculations described by Reid and Hobbs [1998]. Heating of the incoming aerosol by the PCASP ensured that the relative humidity was  $<35\%$ . Because the hygroscopicity of smoke particles was small, the difference in dry and ambient particle sizes was probably  $<10\%$ .

The PCASP number distribution was parameterized by a lognormal curve fit:

$$dN = \frac{1}{\sqrt{2\pi} \ln \sigma_{gc}} \exp \left[ -\frac{(\ln d_p - \ln \text{CMD})^2}{2(\ln \sigma_{gc})^2} \right] d(\ln d_p), \quad (6)$$

where  $d_p$  is the particle diameter, CMD the count median diameter, and  $\sigma_{gc}$  the geometric standard deviation. A similar expression was used to parameterize the particle VMD and the geometric standard deviation of the volume distribution,  $\sigma_{gv}$ .

Particle size spectra were also measured on the UW C-131A using a differential mobility particle sizer (DMPS). The DMPS yielded particle sizes and geometric standard deviations that were consistently larger than those measured by the PCASP [Reid *et al.*, 1998a]. For example, the VMD and  $\sigma_{gv}$  from the DMPS was  $\sim 0.05$   $\mu\text{m}$  and 0.4 greater (respectively) than that derived from the PCASP. The “true” particle size was probably bounded by the values given by the two probes. Because the PCASP operated continuously during the SCAR-B study, the size spectra used in this study are exclusively from the PCASP. However, we use the PCASP data to determine only the variability in particle size spectra, the true particle sizes and geometric standard deviations may be greater than those obtained from the PCASP by as much as 0.05  $\mu\text{m}$  and 0.3, respectively.

## 4. Results

In this paper, in situ measurements obtained aboard the UW C-131A in Brazil are correlated with AOT data from the AERONET Sun photometers. The C-131A made 10 flights near three Sun photometer locations: Cuiabá (15.6°S, 56.1°W), Pantanal (16.4°S, 56.6°W, 100 km SW of Cuiabá), and the Jamari/Pototsi Mine/Repressa Samuel group ( $\sim 9^\circ\text{S}$ ,  $\sim 63^\circ\text{W}$ , 100 km ESE of Porto Velho). The flights and Sun photometer sites used are listed in Table 1.

Complete vertical profiles over the Sun photometer sites were performed on seven of the flights and within  $\pm 1$  hour of the ground-based measurements. On the remaining three flights the airborne data used in this paper were obtained at  $\sim 800$  mbar within  $\pm 1$  hour and 20 km of a Sun photometer measurement. Because the smoke-dominated hazes in Brazil were generally well mixed in the vertical, measurements at  $\sim 800$  mbar are usually good indicators of the intensive properties of the smoke particles over the Sun photometers under clear-sky conditions. Also, the UW C-131A data suggested that the smoke plumes were typically well mixed in the horizontal up to distances of about  $\pm 30$  km. Finally, comparisons of the Ångström coefficient ( $\alpha$ ) derived from measurements with the 3- $\lambda$  nephelometer and the Sun photometer showed that the same air mass was observed in both measurement sets.

Figure 2 shows  $\alpha$  derived from Sun photometer AOT measurements in the midvisible ( $\lambda = 438\text{--}669$  nm) plotted against  $\alpha$  derived from the airborne in situ scattering coefficients mea-

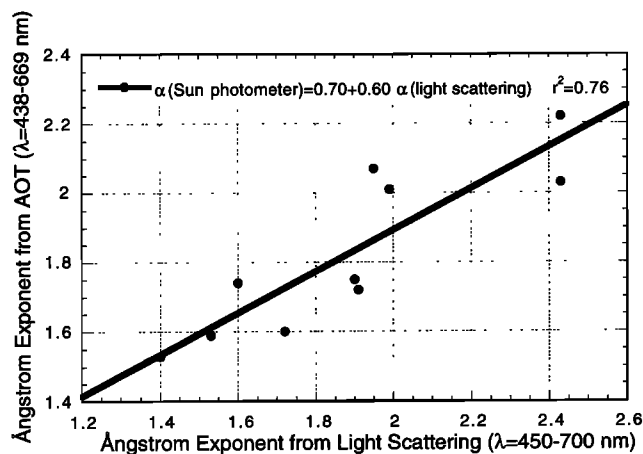


**Figure 2.** Ångström exponent at midvisible wavelengths derived from aerosol optical thickness (AOT) measurements from Aerosol Robotic Network (AERONET) Sun photometers versus the Ångström exponent derived from in situ light-scattering measurements from the 3-λ nephelometer onboard the UW C-131A aircraft.

sured with the 3-λ nephelometer ( $\lambda = 450\text{--}700\text{ nm}$ ). These two variables are well correlated with a regression coefficient ( $r^2$ ) of 0.76; all data points are within 0.2 of the regression line. Variations in the data, while small, must be expected since variations in the wavelength dependence of  $\omega_0$  for smoke aerosols in Brazil can be considerable [Eck et al., 1998]. Additionally, the presence of some coarse particles, which can influence the AOT but are not sampled by the nephelometer, will increase the variability of the data. The good correlation in Figure 2 supports the view that the aerosol properties measured on the C-131A aircraft were from the same airmass as these measured by the Sun photometers.

#### 4.1. Relationship Between the Ångström Exponent and Particle Size Parameters

The Ångström exponents derived from the light-scattering measurements made aboard the UW C-131A aircraft and the AERONET ground-based Sun photometers were strongly correlated with the CMD and VMD of the particles in smoke-dominated hazes over Brazil (Table 2). However, the correlations between  $\alpha$  and the geometric standard deviation for both the CMD and VMD were only fair. The correlation coeffi-

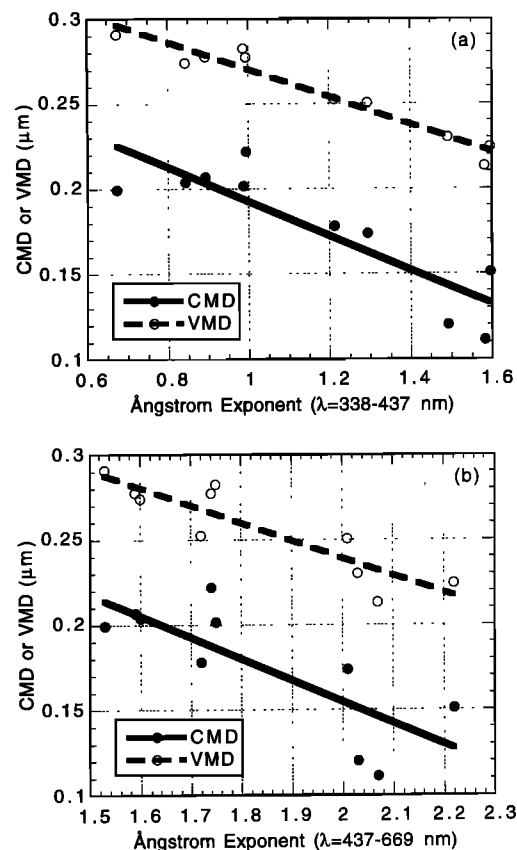


**Figure 3.** Smoke particle count and volume median diameter (CMD and VMD, respectively) versus the Ångström exponent derived from AERONET Sun photometer AOT measurements in the (a) 338–437 nm and (b) 437–669 nm wavelength bands.

cients between  $\alpha$  and the size parameters decreased rapidly as the wavelength interval used for computing  $\alpha$  included longer wavelengths. For example, if the Ångström exponent included the 871- or 1021-nm Sun photometer channels, there were no longer any statistically significant relationships between  $\alpha$  and the particle size parameters.

Regression relationships between the particle median diameters and  $\alpha$  are shown in Figure 3. Figure 3a shows a strong relationship between  $\alpha$  for the 338–437 nm wavelength band

**Table 2.** Correlation Coefficients and  $p$  Values of Particle Size Parameters Derived From In Situ PCASP Measurements Aboard the UW C-131A Aircraft Versus the Ångström Exponent Derived From Sun Photometer AOT Data and the Light-Scattering Measurements From the UW C-131A

Ångström Exponent	CMD	$\sigma_{gc}$	VMD	$\sigma_{gv}$
<i>Sun Photometer AOT</i>				
$\lambda = 338\text{--}437\text{ nm}$	−0.86 (0.00)	0.49 (0.15)	−0.97 (0.00)	0.76 (0.01)
$\lambda = 437\text{--}669\text{ nm}$	−0.78 (0.01)	0.40 (0.25)	−0.89 (0.00)	0.67 (0.03)
$\lambda = 498\text{--}871\text{ nm}$	0.46 (0.17)	−0.07 (0.86)	0.30 (0.39)	−0.30 (0.34)
$\lambda = 338\text{--}1013\text{ nm}$	0.00 (0.99)	−0.41 (0.23)	−0.21 (0.56)	0.10 (0.78)
<i>C-131A Scattering</i>				
$\lambda = 450\text{--}550\text{ nm}$	−0.82 (0.00)	0.55 (0.10)	−0.85 (0.00)	0.62 (0.06)
$\lambda = 450\text{--}700\text{ nm}$	−0.74 (0.01)	0.48 (0.16)	−0.80 (0.00)	0.52 (0.12)
$\lambda = 550\text{--}700\text{ nm}$	−0.62 (0.04)	0.38 (0.27)	−0.70 (0.02)	0.38 (0.28)

Here  $p$  values are in parenthesis. CMD, count median diameter;  $\sigma_{gc}$ , geometric standard deviation of count distribution; VMD, volume median diameter;  $\sigma_{gv}$ , geometric standard deviation of volume distribution.

derived from the Sun photometer measurements and the particle CMD and VMD. Hence,  $\alpha$  is a useful predictor of particle median size in smoke-dominated hazes in Brazil. The regression relations between  $\alpha$  in the 338–437 nm band and the particle distribution parameters are

$$\text{CMD } (\mu\text{m}) = (0.29 \pm 0.02) - (0.10 \pm 0.02) \alpha \quad r^2 = 0.76 \quad (7a)$$

$$\sigma_{gc} = (1.46 \pm 0.10) + (0.14 \pm 0.08) \alpha \quad r^2 = 0.24 \quad (7b)$$

$$\text{VMD } (\mu\text{m}) = (0.35 \pm 0.01) - (0.08 \pm 0.01) \alpha \quad r^2 = 0.94 \quad (7c)$$

$$\sigma_{gv} = (1.14 \pm 0.05) + (1.37 \pm 0.04) \alpha \quad r^2 = 0.58. \quad (7d)$$

Because of the poor correlation between  $\alpha$  and  $\sigma_{gc}$ , it is unlikely that a useful particle number distribution can be determined from  $\alpha$ . However, much of the uncertainty in the particle volume distribution can be reduced if (7c) and (7d) are used. Even so, these equations have some shortcomings. For example, AOT at 338 nm are twice as large as those at mid-visible wavelengths. Consequently, during the biomass burning season in Brazil the 338-nm channel of Sun photometers frequently suffers from a low signal-to-noise problem, especially when the Sun is at high zenith angles. Second, there are relatively few Sun photometers for which  $\alpha$  can be computed at such short wavelengths. Currently, there are no space-borne measurements from which the value of  $\alpha$  can be computed at such short wavelengths (although the MODIS imager on the NASA EOS satellite AM-1 will have channels starting at 412 nm). Fortunately, the regression of the CMD and VMD to  $\alpha$  for the 437–669 nm midvisible range provides useful relationships (Figure 3b):

$$\text{CMD } (\mu\text{m}) = (0.40 \pm 0.06) - (0.13 \pm 0.03) \alpha \quad r^2 = 0.62 \quad (8a)$$

$$\sigma_{gc} = (1.33 \pm 0.2) + (0.16 \pm 0.13) \alpha \quad r^2 = 0.16 \quad (8b)$$

$$\text{VMD } (\mu\text{m}) = (0.44 \pm 0.03) - (0.10 \pm 0.02) \alpha \quad r^2 = 0.80 \quad (8c)$$

$$\sigma_{gv} = (1.00 \pm 0.11) + (0.17 \pm 0.06) \alpha \quad r^2 = 0.45. \quad (8d)$$

As with the 338–437 nm Ångström exponent, the low correlation between  $\alpha$  and  $\sigma_{gc}$  for this case makes it unlikely that a useful particle count distribution can be determined.

For Ångström exponents derived from AOT with wavelengths equal or greater than 871 nm, there are no significant relationships between  $\alpha$  and the particle size parameters (Table 2). For example, in Table 2, not only is there no statistically significant correlation ( $r^2 < 0.21$ ) at the longer wavelengths, but the slope of this regression is of opposite sign to that seen in Figures 3a and 3b. Why do high correlations exist between  $\alpha$  and the particle median diameters for shorter wavelengths only?

Smoke particles in Brazil increase in size owing to coagulation and diffusion-limited processes such as condensation, gas-to-particle conversion, and some cloud processing [Reid et al., 1998a]. If coagulation were the only significant growth process, the geometric standard deviation would remain constant as the particles grew. However, in Brazil the particle geometric standard deviations decrease as particle sizes increase (indicative of diffusion-limited growth). Therefore the growth processes

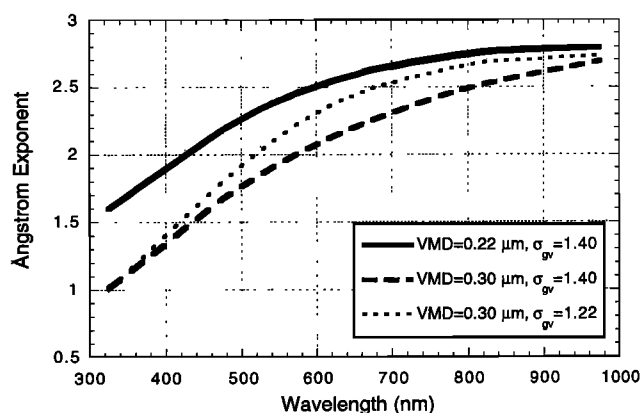


**Figure 4.** Ångström exponent of smoke particles (computed from Mie theory) versus wavelength for three particle volume distributions.

of smoke particles in Brazil probably influence the relationship between  $\alpha$  and particle size.

Figure 4 shows  $\alpha$  (computed from Mie theory assuming a  $\pm 25$  nm bandwidth) versus wavelength for three particle volume distributions. The particles were modeled as layered spheres with a black carbon core comprising 6% of the mass ( $m = 1.8 - 0.6i$ ) and a nonabsorbing shell ( $m = 1.5 - 0i$ ). The youngest smoke measured in regional hazes in Brazil had a PCASP volume distribution parameterized by  $\text{VMD} \approx 0.22 \mu\text{m}$  and  $\sigma_{gv} \approx 1.4$  [Reid et al., 1998a]. Smoke that had aged for several days had a  $\text{VMD} \approx 0.3 \mu\text{m}$  and  $\sigma_{gv} \approx 1.22$ . From Figure 4 we see that the difference between  $\alpha$  for the young and aged smoke decreases as the wavelength increases. At the longer wavelengths,  $\alpha$  differs little between the two size distributions. If the particle size is increased without decreasing the standard deviation ( $\text{VMD} = 0.30 \mu\text{m}$ ,  $\sigma_{gv} = 1.4$ ), the change in  $\alpha$  with VMD is less sensitive to wavelength. Hence the growth law followed by smoke particles in Brazil reduces the information content of the Ångström exponent derived from longer wavelengths.

Coarse mode aerosols in Brazil might also affect the Ångström exponent. The ratio of coarse to fine particle mass during SCAR-B varied anywhere from near zero in the rain forested and broadleaf areas to almost equal partition in the much drier Cerrado region [Ross et al., 1998; Remer et al., 1998]. This coarse mode had a VMD of  $\sim 10 \mu\text{m}$ . If we were to perform Mie calculations on the worst case (equal partition of mass between the two modes), the presence of the coarse mode would reduce the 437–669 nm  $\alpha$  by only  $\sim 0.15$ , whereas the 448–840 nm  $\alpha$  would be reduced by  $\sim 0.3$ . Now, consider Figure 4. At the longer wavelengths, variations in the coarse mode concentration are roughly equal to any variability produced by the fine mode, hence reducing the correlation between  $\alpha$  and fine particle size. In contrast, at shorter wavelengths, variations in  $\alpha$  due to coarse model particles are only about a third that of those produced by changes in the fine mode. As one goes to shorter wavelengths (say the 338–437 nm) the influence of the coarse mode is even less:  $\sim 20\%$ . Hence the variability of an independent coarse mode in Brazil works to disrupt any  $\alpha$ -particle size correlation at longer wavelengths.

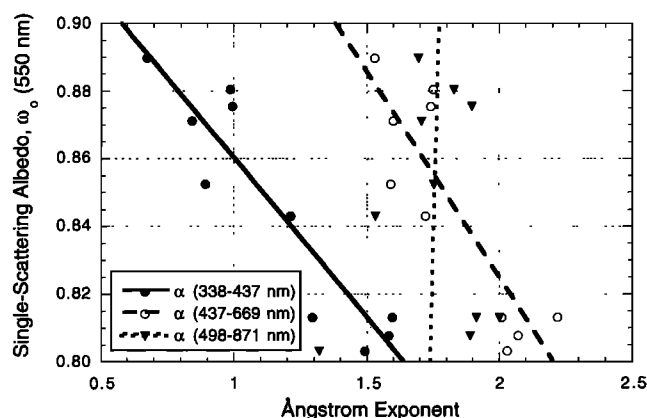


**Figure 5.** Single-scattering albedo of smoke particles versus Ångström exponent ( $\alpha$ ) computed from Sun photometer AOT measurements.

#### 4.2. Relationships Between the Ångström Exponent and Particle Optical Parameters

While the relationships between the Ångström exponent  $\alpha$  and the particle size parameters presented in section 4.1 are interesting, what is most needed are parameterizations that can be used to estimate the optical constants required to model the radiative effects of smoke particles in Brazil. Both the single-scattering albedo and the backscatter ratio were correlated to the Ångström exponent. The single-scattering albedo at 550 nm was found to be well correlated with  $\alpha$  derived over short-wavelength bands (Figure 5):

$$\omega_0 = (0.95 \pm 0.02) - (0.094 \pm 0.014) \alpha_{338-437 \text{ nm}} \quad r^2 = 0.85 \quad (9a)$$

$$\omega_0 = (1.07 \pm 0.05) - (0.122 \pm 0.025) \alpha_{437-669 \text{ nm}} \quad r^2 = 0.75 \quad (9b)$$

Similarly, the backscatter ratio derived from the in situ light-scattering measurements was better correlated to the Ångström exponent at shorter wavelengths (Figure 6). In the case of  $\beta(1)$ , a power law expression provided the best fit:

$$\beta(1)_{450 \text{ nm}} = 0.096 - 0.007 \alpha_{338-437 \text{ nm}}^{4.3} \quad r^2 = 0.72 \quad (10a)$$

$$\beta(1)_{550 \text{ nm}} = 0.093 - 0.014 \alpha_{338-437 \text{ nm}}^{4.0} \quad r^2 = 0.86 \quad (10b)$$

$$\beta(1)_{700 \text{ nm}} = 0.092 - 0.036 \alpha_{338-437 \text{ nm}}^{2.7} \quad r^2 = 0.87 \quad (10c)$$

$$\beta(1)_{450 \text{ nm}} = 0.081 - 0.003 \alpha_{437-669 \text{ nm}}^{3.9} \quad r^2 = 0.58 \quad (11a)$$

$$\beta(1)_{550 \text{ nm}} = 0.093 - 0.001 \alpha_{437-669 \text{ nm}}^{6.0} \quad r^2 = 0.70 \quad (11b)$$

$$\beta(1)_{700 \text{ nm}} = 0.093 - 0.003 \alpha_{437-669 \text{ nm}}^{4.8} \quad r^2 = 0.75. \quad (11c)$$

As in the case of particle size, there was no correlation between  $\omega_0$  or  $\beta(1)$  and  $\alpha$  for wavelength intervals that included the 871- or 1021-nm channels.

Since  $\alpha$  is correlated with particle size, it should also be correlated with the optical properties of the particles. For example, for submicron aerosol particles,  $\beta(1)$  is strongly dependent on particle size. Smoke particles from biomass burning are in a size range in which  $\beta(1)$  from the red-visible wavelengths is particularly sensitive to changes in particle size

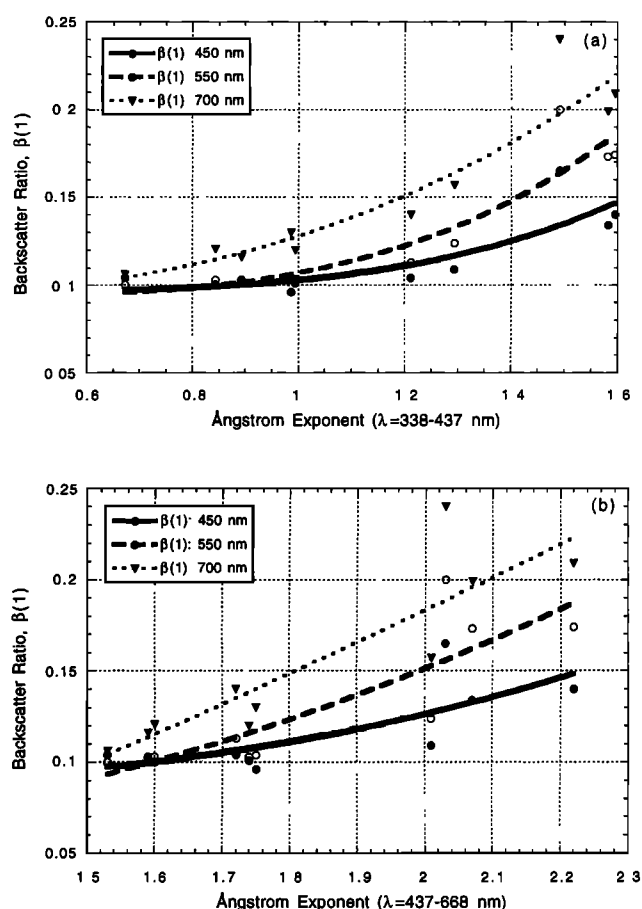


**Figure 6.** Aerosol backscatter ratio,  $\beta(1)$ , versus Ångström exponent computed from Sun photometer AOT measurements for (a) 338–437 nm, and (b) 437–669 nm.

[Reid et al., 1998a, b; Ross et al., 1998]. Hence it is not surprising that  $\alpha$  at shorter wavelengths is best correlated with  $\beta(1)$  at 700 nm. Supporting this, Reid et al. [1998a] found that larger particles in the smoky hazes over Brazil had lower mass absorption efficiencies and higher single-scattering albedos.

#### 4.3. Aerosol Optical Depth as a Confounder

The relationships discussed in sections 4.1 and 4.2 appear to provide useful parameterizations for smoke particle properties. However, the AOT may act as a confounder. The AOT was highly correlated with the Ångström exponents at shorter wavelengths and weakly correlated with  $\alpha$  at longer wavelengths (Figure 7a):

$$\alpha_{338-437 \text{ nm}} = (1.59 \pm 0.07) - (0.33 \pm 0.04) \text{AOT}_{498 \text{ nm}} \quad r^2 = 0.87 \quad (12a)$$

$$\alpha_{437-669 \text{ nm}} = (2.10 \pm 0.08) - (0.21 \pm 0.05) \text{AOT}_{498 \text{ nm}} \quad r^2 = 0.66 \quad (12b)$$

$$\alpha_{498-871 \text{ nm}} = (1.61 \pm 0.25) + (0.12 \pm 0.08) \text{AOT}_{498 \text{ nm}} \quad r^2 = 0.21. \quad (12c)$$

Since AOT is correlated with  $\alpha$ , AOT is correlated with particle size (Figure 7b):



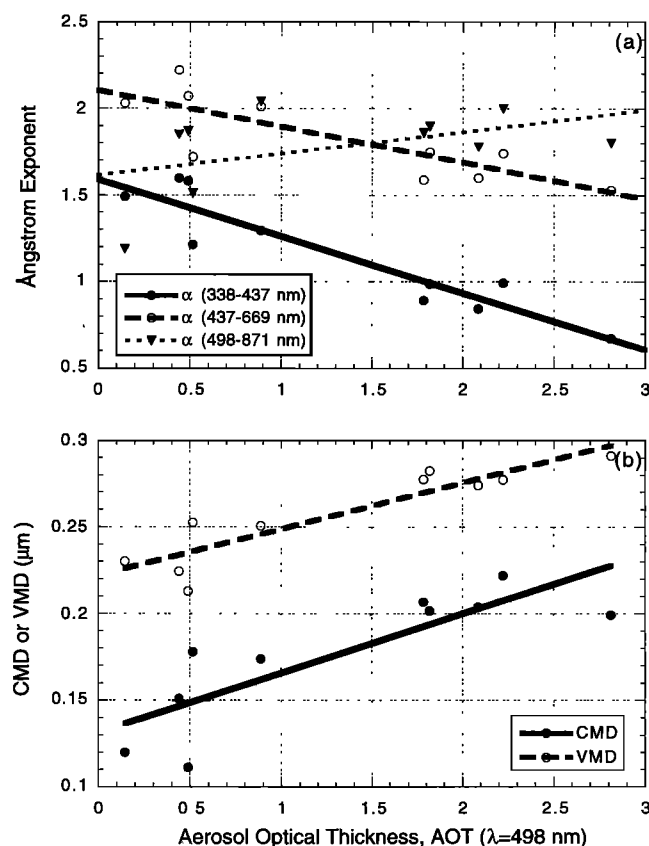


**Figure 7.** (a) Ångström exponent ( $\alpha$ ) and (b) particle count median diameter (CMD) and volume median diameter (VMD) versus aerosol optical thickness (AOT) at  $\lambda = 498$  nm.

$$CMD (\mu\text{m}) = (0.132 \pm 0.013) + (0.034 \pm 0.008) AOT_{498 \text{ nm}} \\ r^2 = 0.69 \quad (13a)$$

$$VMD (\mu\text{m}) = (0.222 \pm 0.007) \\ + (0.027 \pm 0.004) AOT_{498 \text{ nm}} \quad r^2 = 0.82. \quad (13b)$$

Similar correlations exist for AOT at other wavelengths. Part of the reason why this correlation exists is because the regression is between two groups of relatively separate data points. These two groups of points correspond to smoke from burning in the cerrado ( $AOT < 1$ ) and from heavy smoke advected from the forested regions of the Amazon Basin ( $AOT > 1.7$ ). Hence the high correlations seen in Table 2 derive, in part, from a regression between two semi-independent populations.

Despite the AOT being a confounding variable, there is substantial evidence that this problem should not significantly alter the usefulness of equations (9)–(13). First, the regression between  $\alpha$  and AOT is not due to low signal problems in the 339- and 438-nm channels. In all of the cases used in this analysis, the signal intensity levels were at least twice the minimum value acceptable in the AERONET database. In fact, the relationship between  $\alpha$  and AOT appears to hold for cases in which the intensity is 2 orders of magnitude greater than the minimum detectable limits. Second, the regressions of CMD and VMD to  $\alpha$  (for short wavelengths) for the low and high AOT populations independently, yield significant correlations ( $r^2 \approx 0.5$ ). Conversely, significant correlations between CMD (or VMD) and AOT do not exist within each population ( $r^2 <$

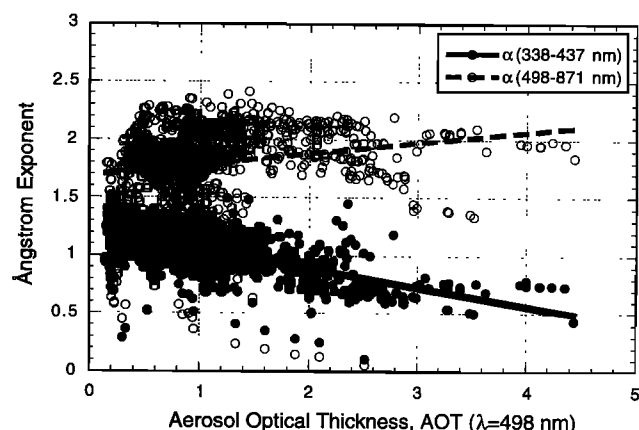


**Figure 8.** Ångström exponent ( $\alpha$ ) versus aerosol optical thickness (AOT) at  $\lambda = 498$  nm from Sun photometer measurements at the Alta Floresta site (August 10 to September 15, 1995).

0.3). This result, together with the theoretical relationship between  $\alpha$  and particle size, suggest that the relationships presented in equations (9)–(13) are valid for most cases.

It is noteworthy that the correlation between the Ångström exponent based on shorter wavelengths and the AOT holds as a general rule for Sun photometer sites in Brazil. For example, for the hourly data at the Alta Floresta Sun photometer site during SCAR-B (Figure 8) the  $\alpha$  calculated over the wavelength range 337–438 nm is correlated with the AOT at 498 nm ( $r^2 = 0.38$ ,  $p = 0.000$ ). However, Ångström exponents that include the 871 nm or longer wavelengths are not correlated with the AOT (e.g.,  $r^2 = 0.1$  for  $\alpha$  based on 498–871 nm). Such trends were observed at most of the Sun photometer sites in Brazil.

The only structure in  $\alpha$  based on the wavelength band 498–871 nm is that at very low AOT ( $AOT < 0.5$ ), where  $\alpha$  tails sharply downward at the lowest AOTs, which is the opposite direction to that for  $\alpha$  at shorter wavelength (Figure 7). This behavior is probably due to the presence of a background coarse-particle mode (recall from section 2 that coarse mode aerosols typically have small values of  $\alpha$ ). As the contribution of fine-mode smoke particles to the AOT increases,  $\alpha$  should increase. Hence the increase of  $\alpha$  for longer wavelengths with AOT at low AOT reflects the transition from a background to a smoky environment.

The relationship between particle concentration (through AOT) and particle size (and hence Ångström exponent) has been observed elsewhere for a variety of fine-mode aerosols [Porter and Clarke, 1997; Remer et al., 1998]. There are several reasons why  $\alpha$  (and particle size) could covary with optical depth in Brazil. (1) The growth rate of the CMD is roughly linearly related to the particle concentration. Hence the particle growth rate is four times greater when the AOT is 2 than when it is 0.5. (2) The growth of the particles by diffusion limited processes (such as condensation) occur more rapidly at higher particle concentrations. (3) Reid and Hobbs [1998] showed that, for the same combustion efficiency, large and intense fires produced larger particles than smaller fires. (4) By growing in size particles, become more efficient light scatterers.

The correlation of  $\alpha$  and other particle properties with AOT does beg the question “Can one use AOT to estimate the intensive properties of particles?” This is essentially the meth-

odology used by *Remer and Kaufman* [1998] in a dynamic aerosol model for the east coast of the United States. Similarly, *Remer et al.* [1998] found a relationship between particle properties, AOT, and precipitable water vapor in Brazil. If no information in the blue or green wavelength regions is available, the use of AOT or other any other extensive parameter as a predictive variable maybe justifiable. However, one must be conscious of the context of such an analysis. It would, in effect, be a regression model on a confounder related to other unmeasured variables (such as transport), rather than on the actual intensive properties of the particles themselves. Hence the use of AOT as a predictor variable may be of some benefit when integrating over long timescales or to gain some qualitative understanding of the climatology of a region, but not on a day-to-day basis.

The correlation of AOT with  $\alpha$  also has a bearing on previous analysis. For example, *Remer et al.* [1998] derived smoke particle size and optical properties from AERONET data in Brazil that had a maximum AOT of 0.503 at 669 nm; this corresponds to an AOT of  $\sim 0.85$  at 498 nm. They chose this cutoff because at higher AOTs the sky becomes less homogeneous and inversions become difficult. Further, the *Nakajima et al.* [1983] code has large errors as AOT approaches 1. However, during the smoke season the AOT at 498 nm at Cuiabá and Jamari is frequently  $>2$ . By confining the calculations to low or moderate AOT, the derived values were likely biased toward smaller smoke particles.

## 5. Applications

The finding that the Ångström exponent of smoke particles in Brazil is correlated with other particle properties can be used to help understand the evolution of smoky hazes over the Amazon Basin. It is known that the properties of smoke particles at emission are significantly different from those that constitute the seasonal smoky hazes that cover much of South America during the biomass burning season [*Reid et al.*, 1998a, b]. However, it is not known on what timescales and length scales the properties of smoke particles change. Specific questions that need to be answered include the following. How rapidly do smoke particles grow? How do the optical properties of smoke particles change spatially and temporally? How large an error is introduced in radiative transfer calculations by modeling smoke particles using static mean values for pertinent optical parameters?

Inversions of Sun photometer almucantar data can be used to infer particle size and scattering phase function [*Nakajima et al.*, 1983, 1996]. Hence, in principle, the questions posed above can be answered using Sun photometer measurements in Brazil. However, useful inversions based on Nakajima et al.'s algorithm from almucantar data can be performed only during periods of relatively low optical depths ( $\tau$  at 669 nm  $< 0.60$ ). This excludes about three quarters of the SCAR-B Sun photometer measurements obtained in Rondonia. Another factor limiting the use of almucantar data is that in SCAR-B the sky was scanned only when the solar zenith angle was  $> 60^\circ$ . Consequently, inversions can be performed only for data collected in the early to mid-morning and late afternoon. Further, at high optical depths the Sun photometers are more prone to low signal problems when the solar zenith angle is high. Compounding these limitations is the impact of clouds on Sun photometer data. Because of these restrictions, almucantar data obtained during SCAR-B is insufficient to answer key

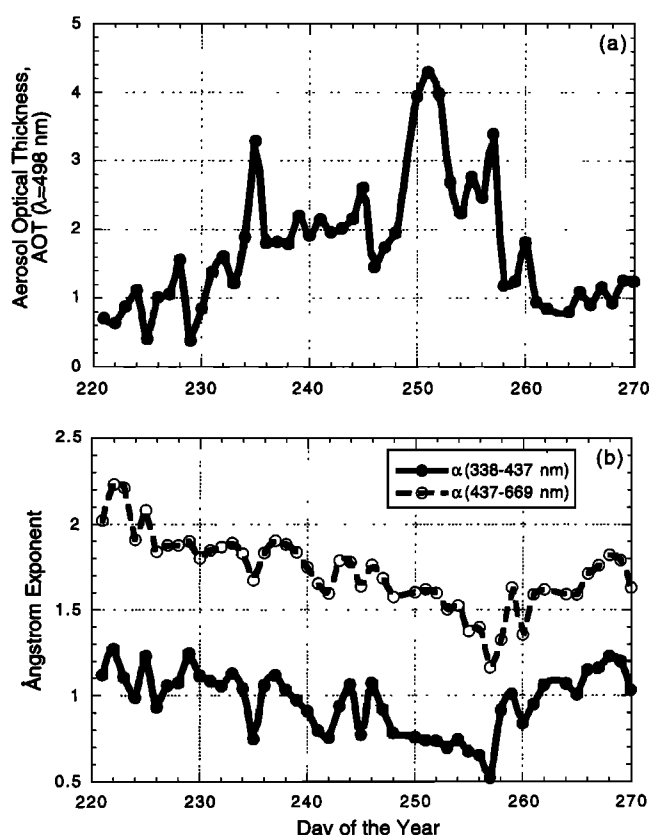


**Figure 9.** Daily-averaged Sun photometer data from the Alta Floresta site. (a) Aerosol optical thickness at  $\lambda = 498$  nm for the 1995 burning season. (b) For the same period, aerosol Ångström exponent ( $\alpha$ ) for the  $\lambda = 338\text{--}437$  nm and  $\lambda = 437\text{--}669$  nm bands.

questions regarding smoke particle evolution. Therefore we must resort to a somewhat cruder analysis based on the more readily available Ångström exponents derived from the Sun photometer data. (Future analysis of almucantar data will use a new algorithm developed by *Dubovik et al.* [1999] which is not limited in the magnitude of the AOT. Also, starting in 1997, almucantar measurements for AERONET were made throughout the day and not limited to solar zenith angles  $> 60^\circ$ . However, if the Dubovik et al. code were used, analysis of the SCAR-B database would still be restricted for many of the reasons discussed above.)

### 5.1. Alta Floresta

The Alta Floresta Sun photometer site in the south central Amazon Basin (latitude =  $9.9^\circ\text{S}$ , longitude =  $56.0^\circ\text{W}$ ) is frequently impacted by smoke during the biomass burning season and it is fairly typical of other sites dominated by heavy smoke in the Amazon Basin [*Artaxo et al.*, 1994]. In addition to strong local sources, smoke advected over Alta Floresta can be generated over a 2500 km fetch. Hence the haze over the site was composed of both local and well-aged smoke. Figures 9a and 9b shows the daily averaged AOT ( $\lambda = 498$  nm) and Ångström exponent (for the 338–437 nm and 437–669 nm wavelength bands) derived from Sun photometer measurements at Alta Floresta during the peak of the 1995 burning season (Julian day 220–270, or August 8 to September 27, 1995). The mid-

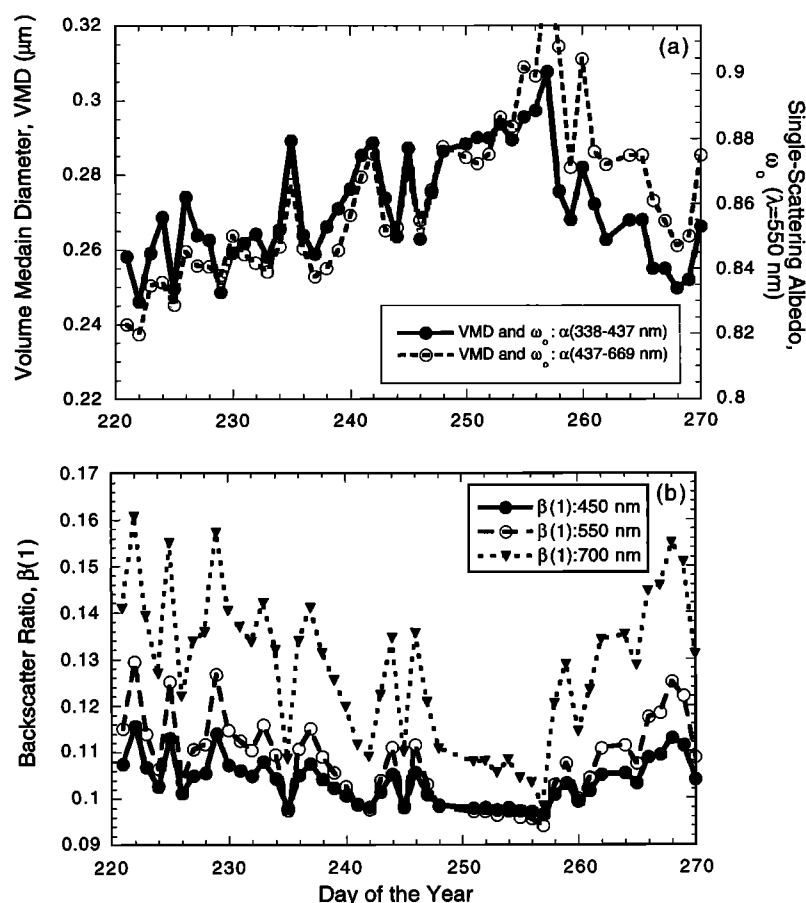


**Figure 10.** (a) Daily-averaged particle volume median diameter (VMD) and single-scattering albedo ( $\omega_0$ ) derived from Sun photometer measurements at the Alta Floresta site as inferred from the  $\lambda = 338\text{--}437$  nm and  $\lambda = 437\text{--}669$  nm Ångström exponents ( $\alpha$ ). (b) Same as Figure 10a, but for particle backscatter ratios at  $\lambda = 450, 550$ , and  $700$  nm as derived from the  $\lambda = 338\text{--}437$  nm Ångström exponent.

visible AOT values at this site varied from 0.5 to 4 during the burning season, with a mean value of  $\sim 1$  (during the SCAR-B study, August 15 to September 15, 1995, AOT averaged 1.5). Since the mass scattering efficiency of particles in the smoky haze was  $\sim 3.5 \text{ m}^2 \text{ g}^{-1}$  [Reid *et al.*, 1998a], the average columnar smoke concentration was  $\sim 0.25 \text{ g m}^{-2}$  at Alta Floresta for the 1995 burning season, and  $0.4 \text{ g m}^{-2}$  during the SCAR-B period.

Over the course of the 1995 burning season,  $\alpha$  varied from 0.5 to 1.3 and from 1.1 to 2.3 for the 338–437 nm and 437–669 nm wavelength bands, respectively. Using equations (7), (8), and (9), the variability in the particle VMD,  $\omega_0$ , and backscatter ratio over the course of the burning season can be determined (Figure 10). Figure 10a shows the daily average values of the VMD and  $\omega_0$  using our regression relations for both the 338–437 nm and 437–669 nm wavelength bands. The inferred VMD and  $\omega_0$  from both of these Ångström exponents track relatively well through the burning season, although at times the two sets of derived values of VMD and  $\omega_0$  differ by as much as  $0.03 \mu\text{m}$  and  $0.03$ , respectively. During SCAR-B, the two sets of derived VMD were within  $0.01 \mu\text{m}$  of each other. After Julian day 270 (September 27, not shown on the graph) the two sets of VMD diverged by as much as  $0.03 \mu\text{m}$ . During this period the AOT was at its lowest, and there was a significant change in particle properties. Late in the burning season the

AOT was probably more strongly influenced by particles other than smoke (e.g., biogenics, dust, and industrial pollutants).

Figure 10 suggests that during the burning season in Brazil particle properties can vary on time scales of  $\sim 3\text{--}30$  days. During the 1995 burning season, the particle VMD at Alta Floresta varied from  $0.23$  to  $0.32 \mu\text{m}$ , with a mean value of  $0.27$  and a standard deviation of  $0.01$  (Figure 10a). Similarly, Figure 10a shows that the single-scattering albedo during the burning season varied from  $0.82$  to  $0.90$ , with a mean value of  $0.86$  and a standard deviation of  $0.02$ . The derived backscatter ratio at  $450, 550$ , and  $700$  nm for the 1995 burning season is more variable at longer wavelengths (Figure 10b). At  $450$  nm,  $\beta(1)$  rarely varied by more than  $\pm 0.01$  from its mean value of  $0.103$ . By contrast,  $\beta(1)$  at  $\lambda = 700$  nm varied dramatically from  $0.10$  to  $0.16$ , with a mean value of  $0.128$ .

The mean values of the VMD,  $\omega_0$ , and  $\beta(1)$  for biomass burning smoke in Brazil discussed above are similar to the mean values reported previously [e.g., Anderson *et al.*, 1996; Reid *et al.*, 1998a; Eck *et al.*, 1998]. Hence the short-term values for these parameters that we have derived are probably representative of mean smoke properties in Brazil.

Figure 10 shows some significant trends over the course of the burning season. While the daily average VMD and  $\omega_0$  usually did not differ significantly between adjoining days (the average VMD and  $\omega_0$  daily rates of change were typically less

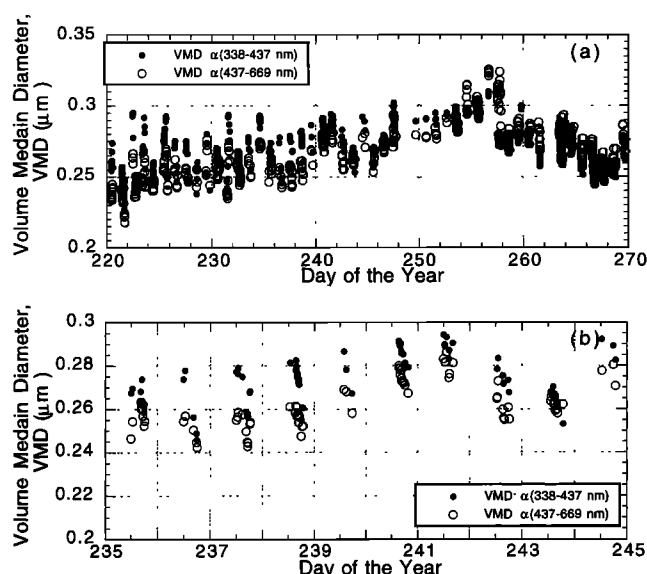


**Figure 11.** (a) Hourly particle volume median diameter, VMD, derived from Sun photometer measurements of the Ångström exponent  $\alpha$  at  $\lambda = 337\text{--}438$  nm (closed circles) and  $\lambda = 438\text{--}668$  nm (open circles). (b) Derived VMD for the middle 20 days of the SCAR-B study.

than  $\pm 0.01 \mu\text{m d}^{-1}$  and  $\pm 0.01 \text{ d}^{-1}$ , respectively), there does appear to be longer-term trends in particle properties. The largest trend in particle properties appears over the course of  $\sim 40$  days, with the maximum in particle size occurring on Julian day 257 (September 14). Over half of the variation in the particle properties can be attributed to this seasonal trend. Interestingly, the form of the dominant trend is similar to the 498 nm AOT pattern in Figure 9a, although there are differences as the maxima in 498 nm AOT and VMD do not match in time. As discussed in section 4.3, there are several reasons to expect an increase in particle size with increasing AOT. Hence it is probable that part of the seasonal trend in particle properties is due to the increase in biomass burning as the burning season progressed. Further, there is the possibility that later in the burning season there was a change in burning from mainly grass and brush to a more forested fuel.

Secondary perturbations in particle properties are also apparent on 3–7 day timescales. These variations are probably due to differences in transport time, plume history (e.g., cloud processing), and possibly source region. Maximum peak-to-trough perturbations in the particle VMD and  $\omega_0$  on weekly timescales are less than  $0.04 \mu\text{m}$  and  $0.05$ , respectively. More typical variations in the VMD and  $\omega_0$  were of the order of  $0.02 \mu\text{m}$  and  $0.02$ , respectively.

Although changes in particle size tended to be small from day to day, changes in  $\alpha$  on an hourly basis suggested that there is a diurnal cycle in particle size in Brazil during the burning season. In Figure 11a we show the derived VMD from the 338–437 nm and 437–669 nm Ångström exponents for all of the hourly data available from the Alta Floresta site. On some days, only a few data points are available owing to cloud screening. From Figure 11a we see that the variability in particle properties through the course of a day can be large. In fact, the variability in particle size through the day is usually larger than the change in the daily averaged particle size. The variability in particle size shows a clear pattern. Figure 11b is

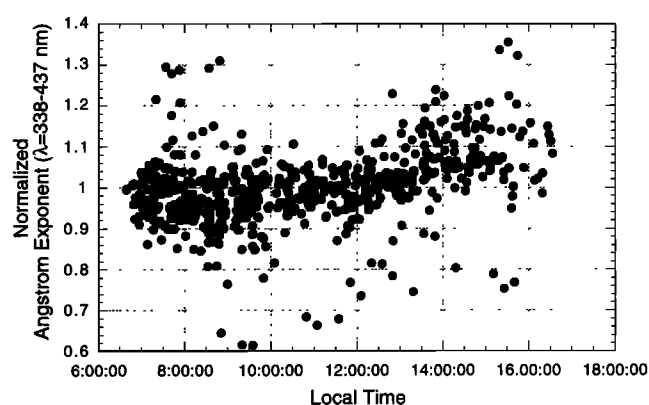


**Figure 12.** Normalized hourly Ångström exponent  $\alpha$  at  $\lambda = 337\text{--}438$  nm versus time of day for the Alta Floresta site during SCAR-B. Each hourly data point was normalized by that day's mean  $\alpha$  value.

an expanded view of Figure 11a for a 10-day period during the middle of the SCAR-B study (Julian day 235–245). From Figure 11a it is apparent that as the day progresses, there is a tendency for the AOT to be influenced by smaller particles (larger values of  $\alpha$ ). The VMD tends to decrease by  $\sim 0.01\text{--}0.03 \mu\text{m}$  through the course of a day. Approximately three-fifths of the days at the Alta Floresta site exhibited increasing Ångström exponents (implying decreasing values of the VMD) as the day progressed (one-fifth of days showed no change through the day, and one-fifth showed VMD increasing through the day). Further, on two-thirds of the days the derived VMD in the morning was greater than the VMD on the previous afternoon. Also, on several occasions, the particle VMD began to rise at the very end of the day, suggesting that the diurnal minimum in VMD occurred around 1500–1800 local time.

The strength of this diurnal pattern in  $\alpha$  (and presumably VMD) is illustrated in Figure 12. Here we present hourly 338–437 nm  $\alpha$  values during the SCAR-B study period that have been normalized by the mean value of  $\alpha$  on that day and plotted versus the time of the day. At  $\sim 1030$  LT,  $\alpha$  begins to increase. Over the course of the day,  $\alpha$  increases by  $\sim 15\%$  (or  $\sim 0.01 \mu\text{m}$  in VMD). The correlation coefficient is statistically significant but low ( $r = 0.3$ ). However, if we perform a 5% trim of outliers,  $r$  increases to  $0.55$ , that is,  $\sim 30\%$  of the daily variance in  $\alpha$  is accounted for by a systematic diurnal cycle. Contrary to this, the AOT does not correlate at all with time of day ( $r = 0.05$ ). While the AOT has considerable diurnal variability (as shown in Table 3), it has no consistent pattern.

It is not surprising that there is a slight diurnal pattern in smoke particle size in Brazil. *Prins et al.* [1998] showed that biomass burning in Brazil has a strong diurnal cycle, with most of the fires being lit in the late morning to midafternoon. Hence particles produced by biomass burning in the afternoon are more likely to be generated from flaming combustion than smoldering combustion. Since particles from flaming combustion tend to be smaller than those generated by smoldering combustion [Reid and Hobbs, 1998], the atmosphere should be enriched by smaller particles in the afternoon. By the early morning of the next day (when the ignition of fires is at a minimum), most of the smoke particles will have aged by at least 12 hours. During the night, smoke particles can grow by coagulation and the condensation of long-chain hydrocarbons

**Table 3.** Statistics of Daily Averaged Haze Properties for the Alta Floresta, Ji Parana, and Cuiabá Sun Photometer Sites

	Cuiabá	Alta Floresta	Ji Parana
Number of Days of Data	49	48	24
<i>AOT (498 nm)</i>			
Site mean $\pm$ standard deviation	$1.0 \pm 0.6$	$1.7 \pm 0.9$	$2.5 \pm 0.7$
(minimum, maximum)	(0.17, 2.5)	(0.40, 4.20)	(1.25, 3.35)
Average daily change ( $\pm$ )	$0.40 \pm 0.36$	$0.46 \pm 0.40$	$0.1 \pm 0.09$
Average diurnal variation ( $\pm$ )	$0.185 \pm 0.15$	$0.53 \pm 0.36$	$0.185 \pm 0.17$
<i>Ångström Exponent (338–437 nm)</i>			
SCAR-B mean $\pm$ standard deviation	$1.08 \pm 0.21$	$0.97 \pm 0.18$	$0.82 \pm 0.15$
Daily averaged (minimum, maximum)	(0.30, 2.13)	(0.52, 1.27)	(0.63, 1.24)
Average daily change ( $\pm$ )	$0.17 \pm 0.13$	$0.12 \pm 0.09$	$0.11 \pm 0.10$
Average diurnal variation ( $\pm$ )	$0.18 \pm 0.15$	$0.13 \pm 0.08$	$0.07 \pm 0.06$
<i>VMD (<math>\mu\text{m}</math>)</i>			
Site mean $\pm$ standard deviation	$0.265 \pm 0.02$	$0.270 \pm 0.01$	$0.285 \pm 0.01$
(minimum, maximum)	(0.23, 0.30)	(0.25, 0.31)	(0.25, 0.30)
Average daily change ( $\pm$ )	$0.013 \pm 0.010$	$0.009 \pm 0.007$	$0.009 \pm 0.008$
Average diurnal variation ( $\pm$ )	$0.015 \pm 0.010$	$0.009 \pm 0.012$	$0.006 \pm 0.010$
<i><math>\omega_0</math> (550 nm)</i>			
Site mean $\pm$ standard deviation	$0.85 \pm 0.02$	$0.86 \pm 0.02$	$0.87 \pm 0.01$
(minimum, maximum)	(0.81, 0.89)	(0.83, 0.90)	(0.83, 0.89)
Average daily change ( $\pm$ )	$0.015 \pm 0.010$	$0.01 \pm 0.010$	$0.01 \pm 0.01$
Average diurnal variation ( $\pm$ )	$0.02 \pm 0.01$	$0.01 \pm 0.015$	$0.01 \pm 0.01$
<i><math>\beta(1)</math> (450 nm)</i>			
Site mean $\pm$ standard deviation	$0.109 \pm 0.010$	$0.103 \pm 0.004$	$0.102 \pm 0.006$
(minimum, maximum)	(0.097, 0.14)	(0.096, 0.116)	(0.096, 0.123)
<i><math>\beta(1)</math> (550 nm)</i>			
Site mean $\pm$ standard deviation	$0.118 \pm 0.018$	$0.108 \pm 0.010$	$0.104 \pm 0.01$
(minimum, maximum)	(0.095, 0.175)	(0.098, 0.129)	(0.095, 0.143)
<i><math>\beta(1)</math> (700 nm)</i>			
Site mean $\pm$ standard deviation	$0.142$	$0.128 \pm 0.015$	$0.122 \pm 0.019$
(minimum, maximum)	(0.102, 0.21)	(0.103, 0.16)	(0.102, 0.177)

Listed is the number of days used in the analysis (i.e., days without complete cloud cover through the day). Also given are the mean, standard deviation, and standard error for the SCAR-B study period (August 14 to September 17), the daily-averaged minimum and maximum values for the SCAR-B study period, the average change in the daily averaged values per day, and the average standard deviation in the diurnal perturbation.

[Reid et al., 1998a]. Further, as the flaming phase for most fires tends to be short lived, the burning biomass is left to smolder in the very late afternoon and through the night. Hence, by morning the atmosphere should be enriched with larger particles produced by smoldering combustion.

The diurnal change in the particle Ångström exponent implies a change in the single-scattering albedo. Figure 13a and 13b shows the derived  $\omega_0$  for the same time periods as Figure 11a and 11b. Changes in  $\alpha$  throughout the day give rise to a  $\sim 0.01$ – $0.03$  peak-to-trough variation in  $\omega_0$ . This diurnal variation in  $\omega_0$  is due to the same factors described in the previous paragraph. Smoke from local fires lit in early afternoons that exhibit flaming combustion begin to influence the AOT late in the day. Particles from flaming combustion in Brazil have higher black carbon contents, smaller sizes and consequently lower  $\omega_0$  [Reid and Hobbs, 1998]. Hence  $\omega_0$  should decrease as the day progresses. In the mornings, most locally generated smoke is from smoldering combustion, which has a lower black carbon content and therefore absorbs less radiation. Also, the smoke transported over a site in the morning will generally have aged for at least 12 h, during which time the particles will have grown by coagulation (which would increase  $\omega_0$ ) and by condensation (which also increases  $\omega_0$  by diluting the black carbon content of the particles).

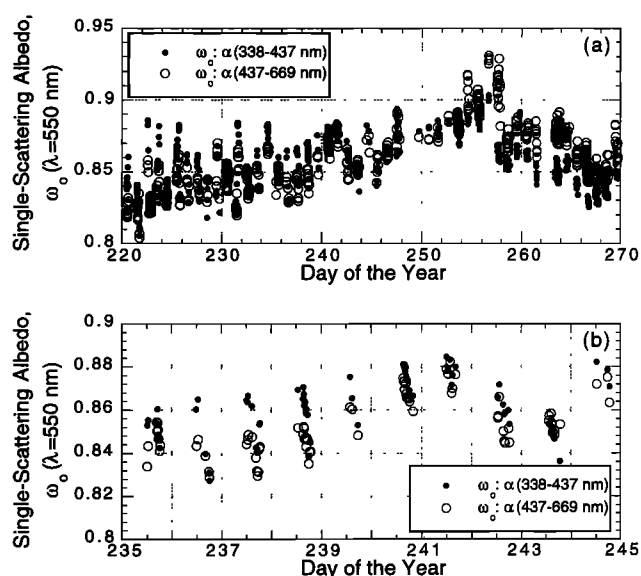


**Figure 13.** (a) Hourly single-scattering albedos derived from Sun photometer measurements at the Alta Floresta site during SCAR-B. (b) Same as Figure 13a but for the middle 20 days of the SCAR-B data.

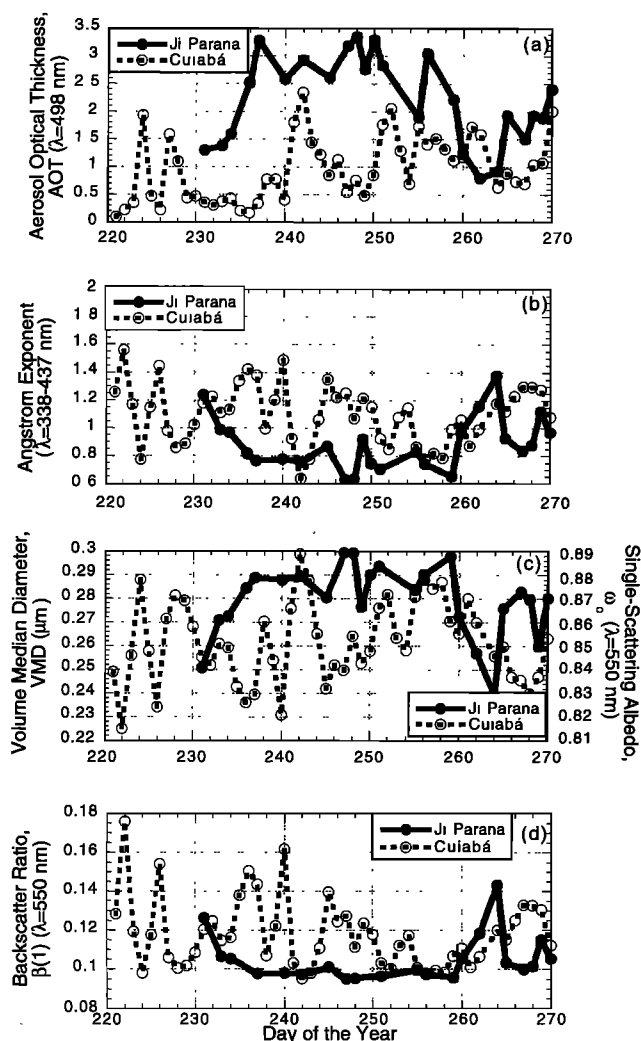


**Figure 14.** Particle properties above the Ji Parana and Cuiabá Sun photometer sites; all data points used are shown. For the Ji Parana site, daily averages could be generated on only half of the days due to low signal (i.e., high  $\tau$  and high optical airmass), clouds, or the large temporal variability of the AOT. (a) Aerosol optical depth ( $\lambda = 550$  nm), (b) 338–437 nm Ångström exponent, (c) particle volume median diameter and  $\omega_0$  at  $\lambda = 550$  nm inferred from  $\alpha$  for  $\lambda = 338$ –437 nm, and (d) same as Figure 14c but for  $\beta(1)$  at  $\lambda = 550$  nm.

## 5.2. Ji Parana and Cuiabá Sun Photometer Sites

The Sun photometer data from Cuiabá and Ji Parana were analyzed in the same way as that described above for the Alta Floresta site. The Alta Floresta, Ji Parana, and Cuiabá sites were the only ones significantly impacted by smoke in the Amazon Basin that were operational during all of the 1995 burning season. Daily averaged values of the AOT (at  $\lambda = 550$  nm), the Ångström exponent (from 338–437 nm), the VMD,  $\omega_0$  (550 nm), and  $\beta(1)$  (550 nm) from the Ji Parana and Cuiabá sites are shown in Figure 14. A summary of our analysis of all three Sun photometer sites is given in Table 3.

The Ji Parana site (latitude  $-10.9^\circ$ , longitude  $-61.8^\circ$ ) was located in the Brazilian state of Rondonia,  $\sim 100$  km south east of the city of Porto Velho, and  $\sim 1200$  km west of the Alta Floresta site. The haze over Ji Parana was from fires in farm, pasture, and rain-forested areas and includes both local and

aged smoke. Optical depths at Ji Parana were very high, averaging 2.5 for the quality and cloud-screened data points. This value of the AOT is a lower limit because about a quarter of the data from this site was unusable due to low signal problems (i.e., the AOT was too high, or the product of  $\tau$  and optical airmass (path length) was so high, that the counts on the Sun photometer were below detectable limits), temporal variability of AOT, and clouds.

The properties of smoke particles over the Ji Parana did not appear to be as variable as those over Alta Floresta (although it should be noted that there was less data available at Ji Parana than Alta Floresta and hence the variability listed in Table 3 should be considered a lower limit). The largest feature at Ji Parana was a 25-day data plateau in the middle of the study period. For these days, the daily averaged particle VMD,  $\omega_0$  (550 nm), and  $\beta(1)$  (550 nm) did not vary by more than  $\pm 0.01$   $\mu\text{m}$ , 0.01, and 0.007, respectively.

As in the case of the Alta Floresta site, a diurnal cycle was detected at Ji Parana, although of half the amplitude. The VMD and  $\omega_0$  at Ji Parana had diurnal variations of 0.009  $\mu\text{m}$  and 0.01, respectively. Because many data points in the early morning and late afternoon were lost due to low signal problems, these diurnal variations are probably lower limits.

The smoke particles over Ji Parana were slightly larger than those over Alta Floresta at statistically significant levels. On average, the smoke over Ji Parana had inferred VMD and  $\omega_0$  values of 0.015  $\mu\text{m}$  and 0.014, respectively, greater than those over Alta Floresta. Considering that these two sites are 600 km apart, and the mean PBL wind was easterly at  $10 \text{ m s}^{-1}$  during this period [Prins *et al.*, 1998], it would take  $\sim 17$  hour for smoke to travel between the sites. This implies that at a minimum, the particle VMD grew at a rate of  $0.02 \mu\text{m d}^{-1}$ . A growth rate of this magnitude can be achieved by coagulation [Reid *et al.*, 1998a]. However, Prins *et al.* [1998] showed that there was extensive burning within 200 km of the Ji Parana site, and this region is one of the largest and most concentrated regions of biomass burning in Brazil. This suggests that the growth rate of particles is  $\sim 0.03$ – $0.04 \mu\text{m d}^{-1}$ , a rate that is somewhat harder to explain by coagulation alone. Reid *et al.* [1998a] suggested that part of this growth rate can be explained by various forms of gas-to-particle conversion. An increase of 0.01  $\mu\text{m}$  in the VMD from gas-to-particle conversion would imply a 10% mass increase during aging, which is well within the mass growth rate of 20–40% suggested by Reid *et al.* [1998a].

The Cuiabá site (latitude,  $-15.5^\circ$ ; longitude,  $-56.0^\circ$ ) was located in the state of Mato Grosso in the cerrado region of Brazil (a mosaic of grassland, scrub, and brush forest). Unlike the Alta Floresta and Ji Parana sites, the properties of smoke particles over Cuiabá were highly variable on 2–5 day time-scales. Cuiabá was the only site where the 3–5 day variability in smoke particle properties was greater than the seasonal trend. Cuiabá was generally on the eastern edge of the subcontinental smoke plume from the burning of the broadleaf forests to the north. Consequently, the AOT was roughly half that at the other sites (mean AOT 1.0). The haze over the Cuiabá site during the early part of the 1995 burning season tended to be from local cerrado and grass fires. However, as the season progressed, the Cuiabá site was more frequently influenced by well aged smoke transported from biomass burning in the broadleaf-forested regions to the north. This transport modulated the AOT and smoke particle size. The increase in particle size associated with the aged smoke was due not only to aging,

but because the smoke from local cerrado fires tended to have a higher proportion of flaming combustion. Hence local smoke from the cerrado region had smaller particles sizes and lower single-scattering albedos than the particles produced in the broadleaf forested regions in the north.

Cuiabá had larger diurnal variations in smoke particle properties than those observed at Alta Floresta or Ji Parana. Particle VMD and  $\omega_0$  for Cuiabá varied, on average, from peak to trough by 0.03  $\mu\text{m}$  and 0.03, respectively, over the course of a day. This finding is not unexpected, since the burning of the scrub and brush foliage of cerrado region is dominated by flaming combustion. As for the Alta Floresta site (see section 5.1), particles produced from flaming combustion in the afternoon begins to influence the total AOT of the hazes. By the next morning, particles over the site would have aged for at least 8 h. However, when the region was significantly influenced by well-aged smoke from the north ( $\text{AOT} > 1$ ), the amplitude of the diurnal variation was diminished by roughly one half.

## 6. Implications for Climate and Remote Sensing Studies

*Liou et al.* [1995] noted that in Africa the Ångström exponent decreases as smoke particles age (in agreement with particle growth during aging). However, in the past, studies such as this have not used the Ångström exponent in any quantitative way. This is because the relationship between the Ångström exponent and particle size varies considerably for different aerosol types (sulfate, smoke, dust, etc.). In the present study, the AOT was dominated by a single aerosol type, namely, biomass smoke. Under these conditions we have demonstrated that the Ångström exponent, for short wavelengths, can be used to estimate the variability of properties of smoke particles.

Smoke aerosols from tropical biomass burning have large regional [Artaxo et al., 1994; Anderson et al., 1996; Ross et al., 1998; Christopher et al., 1996] and possibly global radiative impacts [Hobbs et al., 1997b]. To estimate the direct radiative forcing (DRF) of biomass burning aerosols, it is necessary to characterize their microphysical properties. The two most important parameters that govern the DRF, both at the top of atmosphere (TOA) and at the surface, are the single-scattering albedo ( $\omega_0$ ) and the AOT [Chylek and Coakley, 1974; Hansen et al., 1997; Christopher et al., 1999]. Two approaches can be used to calculate the DRF of smoke aerosols. (1) Using surface measured values of AOT along with knowledge of  $\omega_0$ , broadband radiative transfer calculations can be performed to obtain DRF. However, this method is constrained to those regions where AOT measurements are available. (2) The AOT can be determined from a combination of satellite data, a knowledge of the aerosol optical and physical properties, and model calculations. The normal approach is to assume a log-normal aerosol size distribution together with reasonable values for the real and imaginary parts of the aerosol refractive index and perform Mie calculations to obtain the phase function, single-scattering albedo, and extinction coefficients at visible wavelengths (e.g., 0.58–0.68  $\mu\text{m}$ , channel 1 of AVHRR). These values are then used in a radiative transfer model, such as discrete ordinate, to construct tables that relate calculated radiance values to AOT for a range of Sun-satellite viewing geometries. The discrete ordinate calculations assume plane-parallel geometry, which also requires a surface albedo. Al-

though the AOT at visible wavelengths is required, it is equally important to obtain the AOT over the entire shortwave spectrum for broadband radiative fluxes. Once AOT values are obtained at a particular wavelength, the extinction coefficients at other wavelengths can be used to estimate AOT at other wavelengths.

The results of the present study raises two questions relevant to determining DRF due to aerosols from biomass burning. Does the variability in smoke particle properties have a significant effect on long-term measurements of the albedo of the Earth measured at the TOA? What errors does the variability in smoke properties, introduce into the retrieval of AOT from satellite measurements?

Using a delta-four stream broadband radiative transfer model [Fu and Liou, 1993], downward shortwave irradiance (DSWI) calculations were compared with surface pyranometer measurements at several sites during SCAR-B [Christopher et al., 1999]. It was found that when the AOT and  $\omega_0$  were known, the root mean square (rms) differences between the measurements and calculations were within 20  $\text{W m}^{-2}$ . However, when “static” mean values of  $\omega_0$  were assumed, the rms differences were as large as 100  $\text{W m}^{-2}$  over a day, even when the AOT values were known. This illustrates the sensitivity of DSWI calculations to the assumed value of  $\omega_0$ .

Figure 15 shows the TOA albedo (200–4000 nm) from radiative calculations for two different broadband surface albedos [Charlock et al., 1989] and three  $\omega_0$  values (at  $\lambda = 550 \text{ nm}$ ). The solar zenith angle is 30° and nadir-viewing conditions are assumed. For a surface albedo typical of tropical rain forests (Figure 15a), as AOT increases the TOA albedo shows a corresponding increase. However, the rate of increase is directly dependent upon the single-scattering albedo. For example, for an AOT of 2, the TOA albedo changes from 12–15.5% as  $\omega_0$  changes from 0.80 to 0.90. A 5% change in TOA albedo for this solar zenith angle is equivalent to a shortwave forcing of about  $-60 \text{ W m}^{-2}$  (a negative value denotes that the aerosols reflect more than the underlying background). Figure 15b shows that for a surface albedo typical of cerrado (grass/savanna), the TOA albedo for clear-sky regions is larger than the corresponding values for aerosols, which leads to positive DRF values at the TOA. In this case, the net effect of changing the value of  $\omega_0$  from 0.90 to 0.80 at an AOT of 2 results in a difference in calculated shortwave forcing of  $+55 \text{ W m}^{-2}$ .

While an error of  $\sim 60 \text{ W m}^{-2}$  in shortwave flux due to the variability in smoke particles seems large, the shapes of the curves in Figure 15 need to be considered. For a mean value of  $\omega_0$  of 0.85 and a AOT of 2, if  $\omega_0$  varies by +0.05 and  $-0.05$  the effects on TOA albedo are approximately +0.022 and  $-0.020$ , respectively. Hence, despite the nonlinear shapes of the curves in Figure 15, the impact on TOA albedo at a given AOT is almost symmetric in  $\omega_0$ . Consequently, if the TOA albedo were monitored over a long period of time, the day-to-day variability in smoke particle properties could average out.

The second question is concerned with the inverse problem: given a TOA radiance from a satellite measurement (from which the TOA albedo can be calculated) what is the accuracy of the derived AOT. In Figure 16 the TOA albedo (at 550 nm) is plotted against the AOT (at 550 nm) for a range of single-scattering albedos that we measured in SCAR-B ( $\omega_0 = 0.80$ –0.90). Calculations were performed using the same model as that used to obtain the results shown in Figure 15, except that a mean surface albedo of 0.10 for between rain forest and cerrado regions [Charlock et al., 1989]. Suppose a satellite

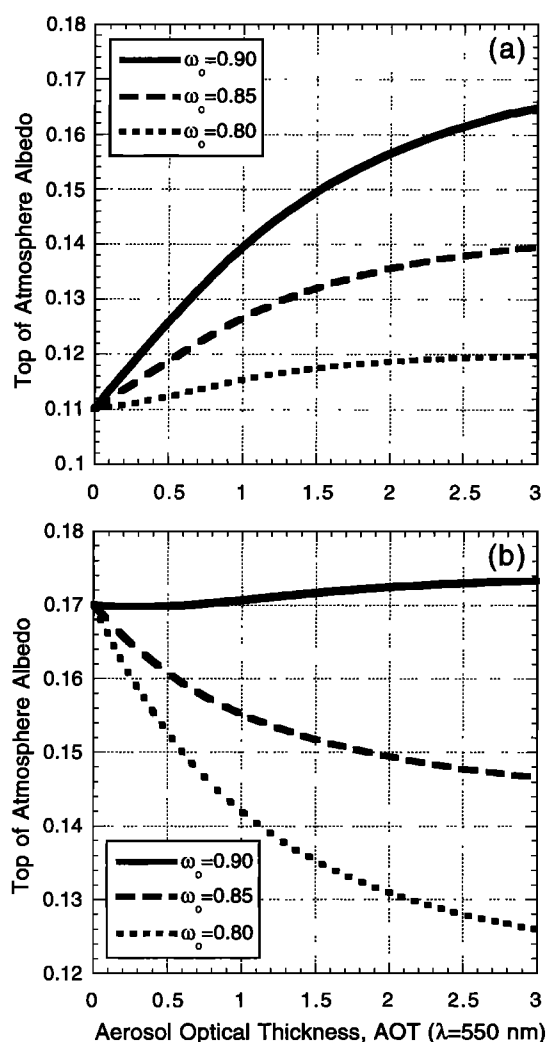


**Figure 15.** Broadband visible, four-stream radiation calculations of TOA albedo as a function of AOT for three values of the single-scattering albedos. Calculations are shown for aerosols over (a) tropical rain forest and (b) grass/savanna and seasonal woods (cerrado). The calculations were performed assuming a  $30^\circ$  solar zenith angle.

measures a TOA albedo of 0.13 for a smoke layer in Brazil, and that an investigator assumes a value for  $\omega_0$  of 0.85. This would result in a derived AOT of 1. However, if the single-scattering albedo of the smoke layer was, in fact, 0.90, the actual AOT would have been 0.7. Worse still, if the actual value of  $\omega_0$  for the smoke layer was 0.80, the true AOT would have been 1.8. Because of the shape of the curves in Figure 16, the sensitivity of the derived AOT from TOA albedo measurements increases as the TOA albedo increases. In Brazil, where AOT are frequently greater than 2, the day-to-day variability in smoke particle properties can result in very large errors in AOT values derived from satellite. Further, because an over-prediction of  $\omega_0$  induces a much larger error in AOT than does an underprediction of  $\omega_0$ , averaging over longer spatial and temporal scales results in derived values of the AOT that are too high.

In view of the sensitivity of derived AOT values to the assumed value of  $\omega_0$ , it is imperative to obtain realistic esti-

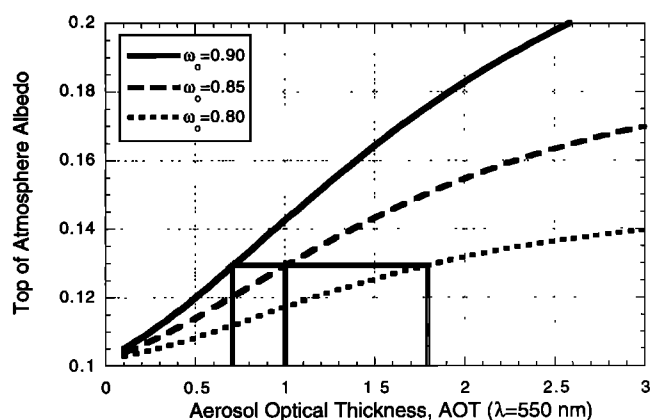


**Figure 16.** Four-stream radiation calculations of the albedo at the TOA as a function of AOT for three values of the single-scattering albedo. Calculations are for a wavelength of 550 nm, a solar zenith angle of  $30^\circ$ , and a surface albedo of 0.10. Also shown is the range of AOT that can be derived for a given TOA albedo.

mates of  $\omega_0$  at high spatial and temporal resolution. Our use of the Ångström coefficient to estimate  $\omega_0$  is one of the first attempts to characterize the variability of smoke aerosol properties. Nakajima and Higurashi [1998] showed that the Ångström exponent derived from satellite can be used to crudely differentiate between coarse- and fine-mode particles on a global scale. As more wavelength bands become available on satellite platforms, the Ångström exponent will become even more useful, especially if AOT retrievals are performed in an iterative fashion using  $\alpha$ . In particular, the MODIS instrument on the Terra satellite should provide pixel level retrievals of  $\omega_0$  and AOT that can be used to improve estimates of DRF and the climatic impacts of smoke aerosols.

## 7. Summary and Conclusions

We have shown that during the biomass burning season in Brazil, Ångström exponents (at shorter wavelengths) derived from Sun photometer measurements of AOT are well correlated with other aerosol particle properties, such as particle size, single-scattering albedo, and the backscatter ratio. These results are consistent with Mie calculations based on the measured properties of biomass burning aerosols. We have also shown that, as is the case for other aerosol types, the AOT and particle size are well correlated for biomass smoke.

During the SCAR-B field experiment, inversions of almucantar sky radiance data were not available during periods of high AOT and partly cloudy skies. Hence, quantitative studies of the variability of smoke particle size in Brazil could not be obtained from this source. However, we have derived regression relations that predict the particle count median diameter, volume median diameter, single-scattering albedo, and backscatter ratio from values of the 338–437 nm and 437–669 nm Ångström exponents. These relationships were used to infer the evolution of smoke particle sizes and optical parameters in the Amazon Basin from Sun photometer measurements of Ångström exponents. While this methodology would be imprecise if used on an hourly or daily basis, when applied to an entire burning season's worth of data, semi-quantitative esti-



mates of the time scales of particles variability required for climate and remote sensing work can be derived.

From observations of the Ångström exponent at three primary Sun photometer sites in Brazil during the 1995 biomass burning season, it was inferred that particle sizes and optical properties vary on spatial and temporal scales ranging from hours to weeks. The daily averaged particle fine mode volume median diameter and the single-scattering albedo at 550 nm varied by  $\pm 0.05 \mu\text{m}$  and  $\pm 0.05$ , respectively, on 5–15 day timescales. These variations were most likely due to differences in the ages and processing of smoke particles reaching the sites. Diurnal variations in particle properties were also detected.

Variations in particle properties over Brazil may have a significant impact on derivations of AOT from satellite radiance measurements. Because TOA reflectance (and hence radiance) by smoky hazes is strongly dependent on the single-scattering albedo when the AOT rises above 1, even relatively small changes in  $\omega_0$  can produce large changes in derived shortwave radiative forcing. Because the spectral dependence of  $\omega_0$  is mostly unknown, derived AOT values at wavelengths other than the mid-visible are even more uncertain. However, if the radiative impact of smoke particles are modeled using good estimates of the average values of the particle parameters, most of the variations in  $\omega_0$  average out. The variability in  $\omega_0$  has a much stronger effect on AOT values derived from satellite measurements at specific times. In this case, it appears that the use of average values for the properties of the smoke can result in errors in the derived value of the AOT of 40% or more.

**Acknowledgments.** This manuscript is dedicated to the memory of Jack Russell, Chief Engineer for the UW Cloud and Aerosol Research Group (1970–1998). His tireless efforts helped to make SCAR-B and many other CARG field studies successful. The authors are grateful to Ronald Ferek and the UW C-131A flight crew for their help in collecting the data. The helpful comments from the anonymous reviewers are also gratefully acknowledged. This manuscript was supported by the Propagation Division of the Space and Naval Warfare Systems Center-San Diego, United States Navy. AERONET's participation in SCAR-B was supported by Diane Wickland, NASA Headquarters, and Michael King, EOS Project Science Office. The University of Washington's participation in SCAR-B was supported by the following grants: NASA NAGW-3750 and NAG 11709; NSF ATM-9400760, ATM-9412082, and ATM-9408941; NOAA NA37RJ0198AM09 (JISAO contribution number 671); and EPA CR822077.

## References

- Anderson, B. E., W. B. Grant, G. L. Gregory, E. V. Browell, J. E. Collins Jr., D. W. Sachse, D. R. Bagwell, C. H. Hudgins, D. R. Blake, and N. J. Blake, Aerosols from biomass burning over the tropical South Atlantic region: Distributions and impacts, *J. Geophys. Res.*, **101**, 24,117–24,137, 1996.
- Ångström, A., On the atmospheric transmission of Sun radiation and on dust in the air, *Geogr. Ann.*, **12**, 130–159, 1929.
- Artaxo, P., F. Gerab, M. A. Yamasoe, and J. V. Martins, Fine mode aerosol composition at three long term atmospheric monitoring sites in the Amazon Basin, *J. Geophys. Res.*, **99**, 22,857–22,868, 1994.
- Charlock, T. P., F. G. Rose, and K. M. Cattany-Carnes, Cross correlations between the radiation and atmospheric variables in a general circulation and in satellite data, *Mon. Weather Rev.*, **117**, 212–220, 1989.
- Christopher, S. A., D. V. Kliche, J. Chou, and R. M. Welch, First estimates of the radiative forcing of aerosols generated from biomass burning using satellite data, *J. Geophys. Res.*, **101**, 21,265–21,237, 1996.
- Christopher, S. A., X. Li, R. W. Welch, P. V. Hobbs, J. S. Reid, T. F. Eck, and B. Holben, Estimation of downward shortwave irradiances in biomass burning regions during SCAR-B, *J. Appl. Meteor.*, in press, 1999.
- Chylek, P., and J. A. Coakley, Aerosols and climate, *Science*, **183**, 75–77, 1974.
- Dellago, C., and H. Horvath, On the accuracy of the size distribution information obtained from light extinction and scattering measurements, I, Basic considerations and models, *J. Aerosol Sci.*, **24**, 129–141, 1993.
- Dubovik, O., B. N. Holben, M. D. King, A. Smirnov, T. F. Eck, S. Kinne, and I. Slutsker, A flexible inversion algorithm for retrieval of aerosol optical properties from Sun and sky radiance measurements, paper presented at ALPS 99, Meribel, France, Jan. 18–22, 1999.
- Eck, T. F., B. N. Holben, I. Slutsker, and A. Setzer, Measurements of irradiance attenuation and calculation of aerosol single scattering albedo for biomass burning aerosols in Amazonia, *J. Geophys. Res.*, **103**, 31,865–31,877, 1998.
- Fu, O., and K. N. Liou, Parameterization of the radiative properties of cirrus clouds, *J. Atmos. Sci.*, **50**, 2008–2025, 1993.
- Hansen, J., M. Sato, and R. Ruedy, Radiative forcing and climate response, *J. Geophys. Res.*, **102**, 6831–6864, 1997.
- Hegg, D. A., D. S. Covert, M. J. Rood, and P. V. Hobbs, Measurements of aerosol optical properties in marine air, *J. Geophys. Res.*, **101**, 12,893–12,903, 1996.
- Hobbs, P. V., J. S. Reid, J. A. Herring, J. D. Nance, R. E. Weiss, J. L. Ross, D. A. Hegg, R. D. Ottmar, and C. A. Liousse, Particle and trace-gas measurements in the smoke from prescribed burns of forest products in the Pacific Northwest, in *Biomass Burning and Global Change*, edited by J. S. Levine, pp. 697–715, MIT Press, Cambridge, Mass., 1997a.
- Hobbs, P. V., J. S. Reid, R. A. Kotchenruther, R. J. Ferek, and R. Weiss, Direct radiative forcing by smoke from biomass burning, *Science*, **275**, 1776–1778, 1997b.
- Holben, B. N., A. Setzer, T. F. Eck, A. Pereira, and I. Slutsker, Effect of dry season biomass burning on Amazon Basin aerosol concentrations and optical properties, *J. Geophys. Res.*, **101**, 19,465–19,481, 1996.
- Holben, B. N., et al., Automatic Sun and sky scanning radiometer system for network aerosol monitoring, *Remote Sens. Environ.*, **66**, 1–16, 1998.
- Junge, C. E., The size distribution and aging of natural aerosols as determined from electrical and optical measurements in the atmosphere, *J. Meteorol.*, **12**, 13–25, 1955.
- Kaufman, Y. J., et al., Smoke, Clouds and Radiation-Brazil (SCAR-B) experiment, *J. Geophys. Res.*, **103**, 31,783–31,808, 1998.
- Kotchenruther, R., and P. V. Hobbs, Humidification factors of aerosols from biomass burning in Brazil, *J. Geophys. Res.*, **103**, 32,081–32,090, 1998.
- Liousse, C., C. Devaux, F. Dulac, and H. Cachier, Aging of savannah biomass burning aerosols: Consequences on their optical properties, *J. Atmos. Chem.*, **22**, 1–17, 1995.
- Nakajima, T., and A. Higurashi, A use of two-channel radiances for an aerosol characterization from space, *Geophys. Res. Lett.*, **25**, 3815–3818, 1998.
- Nakajima, T., M. Tanaka, and T. Yamauchi, Retrieval of the optical properties of aerosols from aureole and extinction data, *Appl. Opt.*, **22**, 2951–2950, 1983.
- Nakajima, T., M. Tanaka, M. Yamano, M. Shiobara, K. Arai, and Y. Nakanishi, Aerosol optical characteristics in the yellow sand events observed in May, 1982 in Nagasaki, *J. Meteorol. Soc. Jpn.*, **67**, 279–291, 1989.
- Nakajima, T., T. Glauco, R. Rao, P. Boi, Y. J. Kaufman, and B. N. Holben, Use of sky brightness measurements from ground for remote sensing of particulate polydispersions, *Appl. Opt.*, **35**, 2672–2686, 1996.
- Porter, J. N., and A. D. Clarke, Aerosol size distribution models based on in situ measurements, *J. Geophys. Res.*, **102**, 6035–6045, 1997.
- Prins, E. M., J. M. Feltz, W. P. Menzel, and D. E. Ward, An overview of GOES 8 diurnal fire and smoke results for SCAR-B and the 1995 fire season in South America, *J. Geophys. Res.*, **103**, 31,821–31,836, 1998.
- Pueschel, R. F., V. R. Overbeck, K. G. Snetsinger, P. B. Russell, G. V. Ferry, J. C. Wilson, J. M. Livingston, S. Verma, and W. Fong, Calibration correction of an active scattering spectrometer probe to account for the refractive index of stratospheric aerosols, *Aerosol Sci. Tech.*, **12**, 992–1002, 1990.

- Radke, L. F., D. A. Hegg, P. V. Hobbs, and J. E. Penner, Effects of aging on the smoke from a large forest fire, *Atmos. Res.*, **38**, 315–332, 1995.
- Reid, J. S., and P. V. Hobbs, Physical and optical properties of smoke from individual biomass fires in Brazil, *J. Geophys. Res.*, **103**, 32,013–32,031, 1998.
- Reid, J. S., P. V. Hobbs, R. J. Ferek, D. R. Blake, J. V. Martins, M. R. Dunlap, and C. Liousse, Physical, chemical and optical properties of regional hazes dominated by smoke in Brazil, *J. Geophys. Res.*, **103**, 32,059–32,080, 1998a.
- Reid, J. S., P. V. Hobbs, C. Liousse, J. V. Martins, R. E. Weiss, and T. F. Eck, Comparisons of techniques for measuring shortwave absorption and the black carbon content of biomass burning aerosols, *J. Geophys. Res.*, **103**, 32,041–32,050, 1998b.
- Remer, L. A., and Y. J. Kaufman, Dynamical aerosol model: Urban/industrial aerosol, *J. Geophys. Res.*, **103**, 13,859–13,871, 1998.
- Remer, L. A., Y. Kaufman, B. N. Holben, A. M. Thompson, and D. P. McNamara, Biomass burning aerosol size distribution and modeled optical properties, *J. Geophys. Res.*, **103**, 31,879–31,892, 1998.
- Ross, J., P. V. Hobbs, and B. Holben, Radiative characteristics of regional haze dominated by smoke from biomass burning in Brazil: Closure tests and direct radiative forcing, *J. Geophys. Res.*, **103**, 31,925–31,942, 1998.
- Smirnov, A., B. N. Holben, T. F. Eck, O. Dubovik, and I. Slutsker, Cloud screening and quality control algorithms for the AERONET database, *Remote Sens. Environ.*, in press, 1999.
- Tanré, D., C. Devaux, M. Herman, and R. Santer, Radiative properties of desert aerosols by optical ground-based measurements at solar wavelengths, *J. Geophys. Res.*, **93**, 14,223–14,231, 1988.
- Tomasi, C., E. Caroli, and V. Titale, Study of the relationship between Ångström's wavelength exponent and Junge particle size distribution exponent, *J. Clim. Appl. Meteorol.*, **22**, 1707–1716, 1983.
- Westphal, D. L., and O. B. Toon, Simulations of microscale, radiative, and dynamical processes in a continental-scale forest fire smoke plume, *J. Geophys. Res.*, **96**, 22,379–22,400, 1991.
- S. A. Christopher, Department of Atmospheric Science, University of Alabama, Huntsville, AL.
- T. F. Eck, Raytheon RITSS Corporation, Code 923, NASA Goddard Space Flight Center, Greenbelt, MD 20771.
- P. V. Hobbs, Department of Atmospheric Sciences, University of Washington, Seattle, WA.
- B. Holben, NASA Goddard Space Flight Center, Greenbelt, MD 20771.
- J. S. Reid, Tropospheric Branch-D883, Space and Naval Warfare System Center, 49170 Propagation Path, San Diego, CA 92152-7385. (jreid@spawar.navy.mil)

(Received February 25, 1999; revised July 6, 1999; accepted August 4, 1999.)